

Somatostatin subtype 2 receptor-targeted metal-based anticancer complexes

Journal:	<i>Bioconjugate Chemistry</i>
Manuscript ID:	bc-2012-00173h.R2
Manuscript Type:	Article
Date Submitted by the Author:	n/a
Complete List of Authors:	Marchán, Vicente; University of Barcelona, Organic Chemistry Barragán, Flavia; University of Barcelona, Organic and Inorganic Chemistry González, Carlos; Instituto de Química Física, Massaguer, Anna; Universitat de Girona, Dolors, Carrion-Salip; Universitat de Girona, Rafael, de Llorens; Universitat de Girona, Sadler, Peter; University of Warwick, Chemistry Moreno, Virtudes; University of Barcelona, Inorganic Chemistry Gomez-Pinto, Irene; Instituto de Química Física Rocasolano, EEM Alejandro, Gonzalez-Canto; University of Barcelona, Organic and Inorganic Chemistry

SCHOLARONE™
Manuscripts

Somatostatin subtype 2 receptor-targeted metal-based anticancer complexes

Flavia Barragán,^{†,‡,&} Dolors Carrion-Salip,^{§,&} Irene Gómez-Pinto,[⊥] Alejandro González-Cantó,^{†,‡} Peter J. Sadler,[#] Rafael de Llorens,[§] Virtudes Moreno,[‡] Carlos González,[⊥] Anna Massaguer,^{*,§} and Vicente Marchán^{*,†}

[†]*Departament de Química Orgànica and IBUB, Universitat de Barcelona, Martí i Franquès 1-11, E-08028 Barcelona, Spain.*

[‡]*Departament de Química Inorgànica, Universitat de Barcelona, Martí i Franquès 1-11, E-08028 Barcelona, Spain.*

[§]*Departament de Biologia, Universitat de Girona, Campus Montilivi, E-17071 Girona, Spain.*

[⊥]*Instituto de Química-Física “Rocasolano”, CSIC, Serrano 119, E-28006, Madrid, Spain.*

[#]*Department of Chemistry, University of Warwick, Coventry, CV4 7AL, UK.*

E-mail: vmarchan@ub.edu (Vicente Marchán); anna.massaguer@udg.edu (Anna Massaguer).

[&]Both authors contributed equally to this work.

ABSTRACT

1
2
3
4 Conjugates of a dicarba analogue of octreotide, a potent somatostatin agonist whose receptors are
5 overexpressed on tumor cells, with [PtCl₂(dap)] (dap = 1-(carboxylic acid)-1,2-diaminoethane) (**3**), [(η⁶-
6 bip)Os(4-CO₂-pico)Cl] (bip = biphenyl, pico = picolinate) (**4**), [(η⁶-*p*-cym)RuCl(dap)]⁺ (*p*-cym = *p*-
7
8
9
10
11
12
13
14
15
16
17
18
19
20
21
22
23
24
25
26
27
28
29
30
31
32
33
34
35
36
37
38
39
40
41
42
43
44
45
46
47
48
49
50
51
52
53
54
55
56
57
58
59
60
cymene) (**5**), and [(η⁶-*p*-cym)RuCl(imidazole-CO₂H)(PPh₃)]⁺ (**6**), were synthesized by using a solid-
phase approach. Conjugates **3-5** readily underwent hydrolysis and DNA binding whereas conjugate **6**
was inert to ligand substitution. NMR spectroscopy and molecular dynamics calculations showed that
conjugate formation does not perturb the overall peptide structure. Only **6** exhibited antiproliferative
activity in human tumor cells (IC₅₀ = 63 ± 2 μM in MCF-7 cells and IC₅₀ = 26 ± 3 μM in DU-145 cells)
with an active participation of somatostatin receptors in cellular uptake. Similar cytotoxic activity was
found in a normal cell line (IC₅₀ = 45 ± 2.6 μM in CHO cells), which can be attributed to a similar level
of expression of somatostatin subtype-2 receptor. These studies provide new insights into the effect of
receptor-binding peptide conjugation on the activity of metal-based anticancer drugs, and demonstrate
the potential of such hybrid compounds to target tumor cells specifically.

INTRODUCTION

1
2
3 The overexpression of the receptors for many regulatory peptides in human tumor cells in comparison to
4 their expression in normal cells, has prompted research on the use of such peptides in tumor targeting
5 both for diagnostic and therapeutic purposes.^{1,2,3} From the therapeutical point of view, a promising
6 approach for the treatment of cancer consists on the attachment of a cytotoxic drug to a peptide moiety
7 with the aim of improving its activity and bioavailability. This targeted anticancer strategy will result in
8 therapeutic agents with increased tumor selectivity and decreased toxicity in normal tissues.
9

10
11 Among natural receptor-binding peptides, the neuroendocrine hormone somatostatin and its analogues
12 have received much attention because of their high affinity against its five human receptors (sst₁-
13 sst₅).^{1,3,4} These receptors are overexpressed in various major tumor types, including lung, breast,
14 prostate, adrenal and neuroendocrine tumors in comparison with normal tissues.⁵ The successful use of
15 radiolabelled somatostatin for imaging and radionuclide therapy has prompted the development of new
16 cyclic and acyclic analogues with better receptor affinity and higher stability under physiological
17 conditions.⁶
18

19
20 Octreotide,⁷ **1** (Chart 1), a metabolically-stabilized cyclooctapeptide analogue of somatostatin that
21 includes *D*-amino acids to enhance resistance to enzymatic degradation and a cystine bridge to stabilize
22 the pharmacophore β -turn, is particularly interesting because of its high affinity and selectivity for the
23 receptor sst₂,⁶ which is the receptor subtype most frequently found on tumor cells. This selectivity has
24 allowed the development of derivatives such as [¹¹¹In-DTPA]-octreotide and [⁹⁰Y-DOTA-Tyr³]-
25 octreotide which are used in the clinics for molecular imaging and therapy of neuroendocrine tumors,
26 respectively.⁸ Octreotide has also been conjugated to cytotoxic organic compounds such as doxorubicin,
27 camptothecin and paclitaxel, with promising results in some cases because of the reduced toxicity and
28 the increased selectivity of the conjugates compared with that of the free drug.^{4,9}
29
30
31
32
33
34
35
36
37
38
39
40
41
42
43
44
45
46
47
48
49
50
51
52
53
54
55
56
57
58
59
60

1 Despite the successful history of cisplatin and its second-generation derivatives (carboplatin and
2 oxaliplatin) in the treatment of some types of cancer,¹⁰ the severe toxic side-effects and the acquired or
3 intrinsic resistance of certain tumors has focused research on other metal-based complexes in an effort to
4 develop improved chemotherapeutic agents.^{11,12} Indeed, in addition to several platinum compounds, two
5 ruthenium(III) coordination complexes, *trans*-[RuCl₄(DMSO)(Im)]ImH (NAMI-A) and *trans*-
6 [RuCl₄(Ind)₂]IndH (NKP-1339) are currently on clinical trials.^{13,14}

7
8
9
10
11
12
13
14 In recent years, research on bioinorganic chemistry has also been focused on organometallic
15 ruthenium(II) and osmium(II) arene complexes since these compounds have shown promising *in vitro*
16 and *in vivo* anticancer activities, including cell lines that have become resistant to cisplatin.^{15,16,17,18,19}

17
18
19
20
21
22
23
24
25
26
27
28
29
30
31
32
33
34
35
36
37
38
39
40
41
42
43
44
45
46
47
48
49
50
51
52
53
54
55
56
57
58
59
60
Ruthenium and its heavier congener osmium offer several advantages in comparison with platinum
compounds, including the ability to bind to a wide variety of types of ligands, the availability of
additional coordination sites in octahedral complexes, the possibility of controlling the shape of the
complex and the changes in the oxidation state. It is also particularly relevant that they have a capacity
to undergo ligand exchange in a similar way than cisplatin, which makes them particularly attractive for
developing new anticancer drugs. Unlike cisplatin which has two reactive Pt–Cl coordination bonds,
some active organometallic piano-stool complexes have only one reactive site (Ru/Os–Cl). The aquation
of the chlorido complexes, mostly suppressed in extracellular fluids (chloride concentration ~100 mM),
is triggered inside the cell nucleus by the low chloride concentration (4 mM), allowing the interaction of
the active aqua species with biomolecules such as DNA.^{20,21,22}

Based on these precedents, a promising approach in the search of new metal-based anticancer drugs
would consist of the conjugation of platinum and classical non-platinum metal complexes (e.g.
ruthenium and osmium) to carrier molecules such as receptor-binding peptides. Indeed, given the
overexpression of selective receptors for these peptides on the membrane of tumoral cells, it is expected
that the peptide sequences will have a positive effect on the therapeutic properties of the metal-based
drug (e.g. reduction of the toxic side-effects) since they will act as a “tumour-targeting devices”. With
this idea in mind we have synthesized conjugates between a dichloridoplatinum(II) complex and

1 octreotide derivatives in which the disulfide bond had been replaced by CH₂-CH₂ or CH=CH linkages.²³

2 This chemical modification on the peptide does not substantially alter the binding affinity of the dicarba-
3 octreotide analogues for the sst₂ receptor but increases the stability of the carrier biomolecule in the
4 reductive cellular environment.²⁴ In addition, we have recently described the synthesis and DNA
5 ruthenation under visible light irradiation of a photoactivated ruthenium(II) arene complex conjugated to
6 a dicarba analogue of octreotide.²⁵ In recent years, several coordination or organometallic complexes
7 have also been conjugated to carrier molecules such as receptor-binding peptides or known delivery
8 peptides to improve both cellular uptake to cancer cells and cytotoxic activity of the metal-based
9 drug.^{26,27,28,29,30,31,32,33}

10 Herein we report on the use of conjugates between octreotide and several metal complexes as new
11 chemotherapeutic agents. In particular, the synthesis of hybrid compounds between the dicarba analogue
12 of octreotide (**2**) and platinum(II), ruthenium(II) and osmium(II) metal complexes has been
13 accomplished by efficient solid-phase procedures (compounds **3-6** in Chart 1). The influence of the
14 attachment of the metal complex on the structure of octreotide has been studied by NMR spectroscopy
15 and molecular dynamics, as well as the capacity of these conjugates to bind DNA. Finally, cellular
16 uptake and cytotoxicity studies have been carried out in a normal cell line and two human tumoral cell
17 lines.

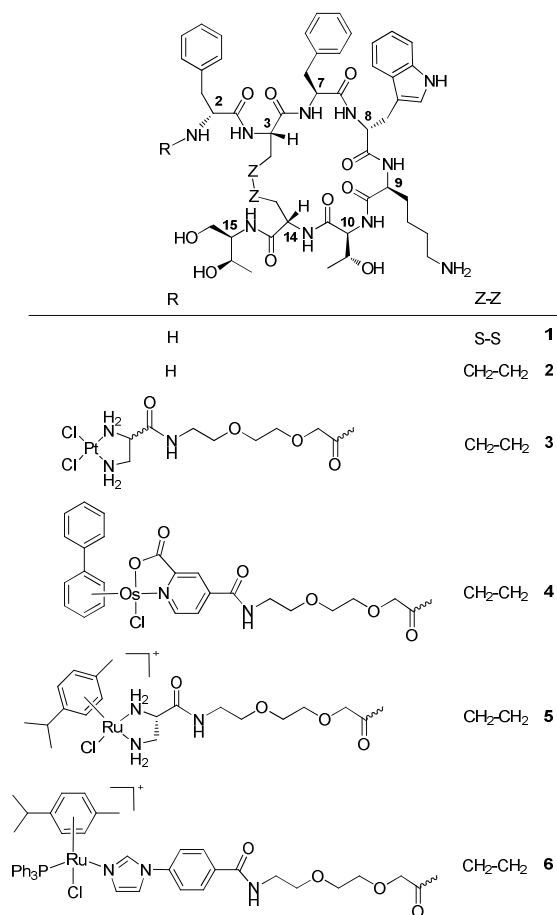


Chart 1. Structure of the conjugates synthesized. Numbering of the amino acid residues follows that of native somatostatin.

EXPERIMENTAL PROCEDURES

Materials and Methods. Unless otherwise stated, common chemicals and solvents (HPLC grade or reagent grade quality) were purchased from commercial sources and used without further purification. Peptide grade DMF was from Scharlau. Fmoc-protected amino acids, resins and coupling reagents for solid phase synthesis were obtained from Novabiochem, Bachem or Iris Biotech. Fmoc-Hag-OH was purchased from Bachem. Fmoc-*L*-threoninol *p*-carboxyacetal was synthesized following previously reported procedures.³⁴ Solid-phase syntheses were performed manually in a polypropylene syringe fitted with a polyethylene disc. Second-generation Grubbs catalyst and Wilkinson's catalyst were purchased from Aldrich. Milli-Q water was directly obtained from a Milli-Q system equipped with a 5000-Da ultrafiltration cartridge. Metal complexes (\pm) -[PtCl₂(dap)] (**7**),²³ (\pm) -[PtCl₂(Etdap)] (**15**),³⁵ [$(\eta^6$ -bip)Os(4-CO₂-pico)Cl] (**8**),³⁶ [$(\eta^6$ -*p*-cym)Ru(μ -Cl)Cl]₂] (**9**), [$(\eta^6$ -*p*-cym)RuCl₂(PPh₃)] (**10**),³⁷ and [$(\eta^6$ -*p*-cym)RuCl(PPh₃)₂][PF₆] (**11**)³⁸ were synthesized and characterized as previously described. (*L*)-2,3-Diaminopropionic acid methyl ester dihydrochloride³⁹ and *N*^α,*N*^β-bis-(9-fluorenylmethyloxycarbonyl)-*L*-2,3-diaminopropionic acid⁴⁰ were synthesised as previously described. 5(6)-Carboxyfluorescein was purchased from Aldrich and octreotide acetate from Bachem. All the assayed compounds displayed a purity $\geq 95\%$, determined by HPLC analysis.

The human breast cancer cell line MCF-7 and the human prostate carcinoma cell line DU-145 were obtained from the American Tissue Culture Collection (ATTC, Rockville, MD, USA). Chinese hamster ovary (CHO) cells were used as non-tumor cell line. The cells were maintained in Dulbecco's modified eagle's medium supplemented with 10% fetal bovine serum and 1% penicillin-streptomycin (GIBCO BRL, Grand Island, NY) at 37 °C in a humidified atmosphere containing 5% CO₂. The cells were passaged two times per week.

NMR spectra were recorded at 25 °C on Varian Gemini 300 MHz and Varian Mercury 400 MHz spectrometers using deuterated solvents. Tetramethylsilane (TMS) was used as an internal reference (δ 0 ppm) for ¹H spectra recorded in CDCl₃ and the residual signal of the solvent (δ 77.16 ppm) for ¹³C

1 spectra. For CD₃OD, acetone-*d*₆, DMSO-*d*₆ or D₂O, the residual signal of the solvent was used as a
2 reference.
3
4

5 High resolution MALDI-TOF mass spectra were recorded on a 4800 Plus MALDI-TOF/TOF
6 spectrometer (Applied Biosystems) in the positive-ion mode using 2,4-dihydroxybenzoic acid as a
7 matrix. ESI mass spectra (ESI-MS) were recorded on a Micromass ZQ instrument with single
8 quadrupole detector coupled to an HPLC. High resolution electrospray mass spectra (HR ESI MS) were
9 obtained on an Agilent 1100 LC/MS-TOF instrument.
10
11
12
13
14
15
16

17 **Synthesis of metal-octreotide conjugates (3-6 and 12) and fluorescein-labelled peptides (13-14).**

18 Solid-phase peptide synthesis was performed on a Rink amide resin-*p*-MBHA (*f* = 0.34 mmol/g, 100-
19 200 mesh) using standard Fmoc/tBu chemistry with the following side-chain protecting groups: Boc (*N*^t-
20 *tert*-butoxycarbonil, tryptophan and *N*^ε-*tert*-butoxycarbonil, lysine), ^tBu (*O*-*tert*-butyl, threonine) and Trt
21 (*S*-trityl, cysteine). The assembly of the dicarba analogue of octreotide was performed as previously
22 described.^{23,24} Briefly, Fmoc-*L*-threoninol *p*-carboxyacetal (1.8 mol equiv) was first coupled using DIPC
23 (1.8 mol equiv) and HOBT (1.8 mol equiv) in anhydrous DMF for 1 h. The following Fmoc-protected
24 amino acids (2.4 mol equiv) were incorporated with HATU (2.3 mol equiv) and DIPEA (4.8 mol equiv)
25 in anhydrous DMF for 1 h. Microwave-assisted ring closing methatesis using second generation Grubbs
26 catalyst and hydrogenation reaction with Wilkinson's catalyst were carried out as previously described.²³
27 Finally, 8-(9-fluorenylmethyloxycarbonyl-amino)-3,6-dioxaoctanoic acid (3 mol equiv) or γ -
28 aminoisobutyric acid (3 mol equiv) were coupled onto the cyclic dicarba analogue of octreotide **2** bound
29 to resin with DIPC (3 mol equiv) and HOAt (3 mol equiv) in anhydrous DMF for 1 h. After removal of
30 the Fmoc group (20% piperidine in DMF) from the Fmoc-protected linker-derivatized dicarba analogue
31 of octreotide bound to resin, coupling or assembly of the metal complexes on the free *N*-terminal end
32 was carried out as indicated for each metal. The reactor was protected from light by covering it with
33 aluminium foil.
34
35
36
37
38
39
40
41
42
43
44
45
46
47
48
49
50
51
52
53
54
55
56
57
58
59
60

Side-chain deprotection and cleavage from the resin was performed simultaneously either with TFA/TIS/H₂O 95:2.5:2.5 (peptides, fluorescein-labelled dicarba octreotide **13** and conjugate **4**), TFA/phenol/H₂O 95:2.5:2.5 (conjugates **3**, **5**, **6** and **12**) or TFA/H₂O/TIS/EDT 94:2.5:2.5:1 (fluorescein-labelled octreotide **14**) for 1 h at room temperature. Most of the TFA was removed by bubbling N₂ into the solution, and the resulting residue was poured onto cold ether to precipitate the target compound.

Analytical reversed-phase HPLC analyses were carried out on a GraceSmart RP C₁₈ column (250x4 mm, 5 μm, flow rate: 1 mL/min), using linear gradients of 0.045% TFA in H₂O (solvent A) and 0.036% TFA in ACN (solvent B). In some cases, small-scale purification was carried out using the same column. Large-scale purification was carried out on a Jupiter Proteo semipreparative column (250 x 10 mm, 10 μm, flow rate: 3-4 mL/min), using linear gradients of 0.1% TFA in H₂O (solvent A) and 0.1% TFA in ACN (solvent B). After several runs, pure fractions were combined and lyophilized.

-Platinum-octreotide conjugate 3: [PtCl₂(dap)] (5 mol equiv) was coupled with DIPC (5 mol equiv) and NHS (10 mol equiv) in anhydrous DMF for 15 h at rt. Overall yield (synthesis + purification): 14%. Characterization: R_t= 14.2 min (analytical gradient: 20 to 60 % in 30 min); HR ESI MS, positive mode: *m/z* 1479.5574 (calcd mass for C₆₀H₈₈Cl₂N₁₃O₁₄Pt [M+H]⁺: 1479.5598); HR MALDI-TOF MS, positive mode: *m/z* 1479.85 (calcd mass for C₆₀H₈₈Cl₂N₁₃O₁₄Pt [M+H]⁺: 1479.5598), *m/z* 1501.87 (calcd mass for C₆₀H₈₇Cl₂N₁₃NaO₁₄Pt [M+Na]⁺: 1501.5418).

-Osmium-octreotide conjugate 4: [(η⁶-bip)Os(4-CO₂-pico)Cl] (5 mol equiv) was coupled with DIPC (5 mol equiv) and HOAt (5 mol equiv) in anhydrous DMF for 3 h at rt. Overall yield (synthesis + purification): 16%. Characterization: R_t= 20.2 min (analytical gradient: 20 to 60 % in 30 min); HR ESI MS, positive mode: *m/z* 1657.6621 (calcd mass for C₇₆H₉₄ClN₁₂O₁₆Os [M+H]⁺: 1657.6214); HR MALDI-TOF MS, positive mode: *m/z* 1679.60 (calcd mass for C₇₆H₉₂ClN₁₂NaO₁₆Os [M+Na]⁺: 1679.6034).

-Ruthenium(dap)-octreotide conjugate 5: N^α,N^β-bis-(9-fluorenylmethyloxycarbonyl)-L-2,3-diaminopropionic acid (4 mol equiv) was coupled with HATU (3.9 mol equiv) in anhydrous DMF in the presence of DIPEA (8 mol equiv) for 1 h at rt. After removal of the Fmoc protecting groups, octreotide-

bound resin was reacted with **9** (3 mol equiv) in the presence of LiCl (6.6 mol equiv) and NEt₃ (7.2 mol equiv) in a DMF/EtOH 9:1 mixture at 100 °C for 1 h under microwave irradiation (40 W). Overall yield (synthesis + purification): 10%. Characterization: R_t= 14.1 min (analytical gradient: 20 to 60 % in 30 min); HR MALDI-TOF MS, positive mode: *m/z* 1448.40 (calcd mass for C₇₀H₁₀₀N₁₃O₁₄Ru [M-Cl-H]⁺: 1448.6556).

-Ruthenium-octreotide conjugate 6: 4-(1*H*-Imidazol-1-yl)benzoic acid (10 mol equiv) was first coupled with DIPC (10 mol equiv) and HOBT (10 mol equiv) in anhydrous DMF for 1 h at rt. Then, imidazole-derivatized peptide-bound resin was reacted with **11** (3 mol equiv) in the presence of LiCl (3.3 mol equiv) and NEt₃ (20 mol equiv) in a DMF/EtOH 9:1 mixture for 8 h at 50 °C. Overall yield (synthesis + purification): 12%. Characterization: R_t= 14.6 min (analytical gradient: 30 to 100 % in 30 min); HR ESI MS, positive mode: *m/z* 1830.7240 (calcd mass for C₉₅H₁₁₆ClN₁₃O₁₄PRu [M]⁺: 1830.7234), *m/z* 915.8672 (calcd mass for C₇₀H₁₀₂ClN₁₃O₁₄Ru [M+H]²⁺: 915.8656); HR MALDI-TOF MS, positive mode: *m/z* 1795.44 (calcd mass for C₉₅H₁₁₅N₁₃O₁₄PRu [M-Cl-H]⁺: 1794.7468).

-Ruthenium-octreotide conjugate 12. Characterization: R_t= 17.7 min (analytical gradient: 30 to 100 % in 30 min); HR ESI MS, positive mode: *m/z* 1768.6863 (calcd mass for C₉₃H₁₁₂ClN₁₃O₁₂PRu [M]⁺: 1768.6867), *m/z* 884.8481 (calcd mass for C₇₀H₁₀₂ClN₁₃O₁₄Ru [M+H]²⁺: 884.8478). The MS data correspond to the dicarba analogue of octreotide with CH=CH linkage.

-Fluorecein-labelled dicarba analogue of octreotide 13: Resin-bound linker-derivatized dicarba analogue of octreotide was allowed to react with 5(6)-carboxyfluorescein (5 mol equiv), DIPC (5 mol equiv) and HOAt (5 mol equiv) in anhydrous DMF for 16 h, protected from light. After filtration and washing, peptide-bound resin was treated with 20% piperidine/DMF (2 x 45 min). Overall yield (synthesis + purification): 40%. Characterization: R_t= 23.3 min (analytical gradient: 20 to 60 % in 30 min); HR ESI MS, positive mode: *m/z* 1486.6572 (calcd mass for C₇₈H₉₂N₁₁O₁₉ [M+H]⁺: 1486.6571).

-Fluorecein-labelled octreotide 14: Linear fluorescein-linker-derivatized octreotide was assembled on a Rink amide resin as described above with minor modifications: Fmoc-Hag-OH was replaced by Fmoc-Cys(Trt)-OH and all Fmoc-protected amino acids, Fmoc-linker-OH and 5(6)-carboxyfluorescein (5 mol

equiv) were coupled with DIPC (5 mol equiv) and HOAt (5 mol equiv) in anhydrous DMF. After treatment with 20% piperidine/DMF (2 x 45 min) and acidic cleavage and deprotection, the linear peptide was dissolved (final concentration *ca.* 1 mM) in an aqueous ammonium hydrogencarbonate solution (5%, pH 7.7) and stirred at room temperature for 72 h (some drops of DMSO and MeOH were added after 24 h to improve solubility as well as to increase the oxidation rate). Overall yield (synthesis + purification): 15%. Characterization: $R_t = 23.5$ min (analytical gradient: 20 to 60 % in 30 min); HR-ESI MS, positive mode: m/z 1522.5673 (calcd mass for $C_{76}H_{88}N_{11}O_{19}S_2 [M+H]^+$: 1522.5699).

Synthesis of metal complexes. $-\left[(\eta^6\text{-}p\text{-cym})RuCl(dap)\right][PF_6]$ (**16**). (*L*)-2,3-Diaminopropionic acid methyl ester dihydrochloride (0.068 g; 0.359 mmol) was reacted with complex **9** (0.1 g; 0.163 mmol) and NEt_3 (513 μ L; 1.63 mmol) in MeOH (15 mL). The mixture was stirred at room temperature for 3 h. The resulting solution was filtered and the volume of the filtrate reduced (to *ca.* 7 mL) in a rotary evaporator. Solid NH_4PF_6 (10 mol equiv) was added to the solution and stirred at room temperature for 4 h. The resulting orange microcrystalline solid was filtered, washed with cold MeOH (10 mL) and dried *in vacuo* (68 mg, 40%). 1H NMR (400 MHz, $DMSO-d_6$) δ (ppm): 1.22 (6H, d, $J=6.8$ Hz), 2.15 (3H, s), 2.16-2.31 (2H, m); 2.7 (1H, sp, $J=6.8$ Hz), 3.02 (1H, br s); 5.04-5.14 (2H, br m), 5.32 (1H, d, $J=5.6$ Hz), 5.46 (1H, d, $J=6$ Hz), 5.63 (1H, d, $J=6$ Hz), 6.67 (1H, d, $J=5.6$ Hz), 5.88-5.97 (2H, br m). $^{13}C\{^1H\}$ NMR (100 MHz, $DMSO-d_6$) δ (ppm): 18.0, 22.5, 30.4, 58.9, 78.6, 79.4, 80.8, 81.2, 95.7, 101.6, 176.8. HR ESI MS, positive mode: m/z 339.0650 (calcd mass for $C_{13}H_{21}N_2O_2Ru [M-Cl-H]^+$: 339.0646). HR ESI MS, negative mode: m/z 373.0228 (calcd mass for $C_{13}H_{20}ClN_2O_2Ru [M-2H]^-$: 373.0255).

$-\left[(\eta^6\text{-}p\text{-cym})RuCl_2(Im\text{-}BzCOOMe)\right]$. A suspension of **9** (200 mg, 0.33 mmol) in 10 mL of DCM was reacted with the methyl ester of the 4-(1*H*-imidazol-1-yl)benzoic acid (1 mol equiv) and stirred at room temperature. Slowly the suspension dissolved and after 4 h diethyl ether was added with stirring to the resulting orange solution until it became turbid. The red microcrystalline product separated was isolated by filtration, washed several times with ether and dried under *vacuo* (165 mg, 50%). 1H NMR (400 MHz, $CDCl_3$) δ (ppm): 1.31 (6H, d, $J=6.8$ Hz), 2.24 (3H, s), 3.03 (1H, sp, $J=6.8$ Hz), 3.95 (3H, s), 5.32 (2H, d, $J=5.4$ Hz), 5.51 (2H, d, $J=5.4$ Hz), 7.32 (1H, s), 7.43 (2H, d, $J=8.4$ Hz), 7.53 (1H, s), 8.14 (2H,

1
2
3
4
5
6
7
8
9
10
11
12
13
14
15
16
17
18
19
20
21
22
23
24
25
26
27
28
29
30
31
32
33
34
35
36
37
38
39
40
41
42
43
44
45
46
47
48
49
50
51
52
53
54
55
56
57
58
59
60

d, $J=8.4$ Hz), 8.38 (s, 1H). $^{13}\text{C}\{^1\text{H}\}$ NMR (100 MHz, CDCl_3) δ (ppm): 20.1, 23.8, 32.2, 54.0, 83.0, 84.0, 100.0, 104.4, 119.9, 122.4, 131.6, 133.1, 135.0, 139.9, 140.9, 167.2.

$-\text{[(}\eta^6\text{-}p\text{-cym)RuCl(Im-BzCOOMe)(PPh}_3\text{)]}[\text{PF}_6\text{}]$ (**17**). Complex $[\text{(}\eta^6\text{-}p\text{-cym)RuCl}_2\text{(Im-BzCOOMe)}]$ (81 mg, 0.16 mmol) was reacted with PPh_3 (1 mol equiv) in methanol (5 mL) for 1 h under reflux. The resulting yellow solution was cooled to room temperature and ammonium hexafluorophosphate (1.1 mol equiv) dissolved methanol (1 mL) was added. A yellow crystalline solid was filtered off and washed several times with methanol and diethyl ether (106 mg, 90%). ^1H NMR (400 MHz, acetone- d_6) δ (ppm): 1.19 (6H, dd, $J=7.2$ Hz), 1.83 (3H, s), 2.60 (1H, sp, $J=7.2$ Hz), 3.93 (3H, s), 5.36 (1H, dt, $J=6$ Hz), 5.87 (1H, d, $J=6$ Hz), 6.07 (1H, d, $J=6$ Hz), 6.20 (1H, d, $J=6$ Hz), 7.44-7.54 (17H, m), 7.65 (2H, dt, $J=10.4$ Hz), 8.15 (2H, d, $J=8.8$ Hz), 8.41 (1H, s). $^{31}\text{P}\{^1\text{H}\}$ NMR (acetone- d_6) δ (ppm): 36.51 (s). $^{13}\text{C}\{^1\text{H}\}$ NMR (100 MHz, acetone- d_6) δ (ppm): 19.1, 22.3, 24.2, 32.7, 53.9, 87.9, 90.2, 90.8, 95.7, 95.8, 105.0, 115.2, 115.3, 121.8, 123.1, 130.2, 130.3, 132.0, 132.1, 132.5, 132.9, 132.8, 133.0, 136.1, 136.2, 141.1, 141.3, 167.1. HR-ESI MS, positive mode: m/z 735.1488 (calcd mass for $\text{C}_{39}\text{H}_{39}\text{ClN}_2\text{O}_2\text{PRu} [\text{M}]^+$: 735,1481), m/z 533.0729 (calcd mass for $\text{C}_{28}\text{H}_{29}\text{ClPRu} [\text{M}-(\text{Im-BzCOOMe})]^+$: 533,0739), m/z 497.0959 (calcd mass for $\text{C}_{28}\text{H}_{28}\text{PRu} [\text{M}-(\text{Im-BzCOOMe})-\text{Cl-H}]^+$: 497.0972).

DNA binding studies. Complexation reactions were carried out in H_2O (4 mM NaCl) at 37 °C. The required volume of an aqueous solution of the corresponding metal-octreotide conjugate was mixed with the required volume of an aqueous solution of $5'$ dCATGGCT (1-2 mol equiv). Regarding conjugate **5**, DNA binding studies were performed with the analogue with the CH=CH linkage isoster of octreotide (denoted as **5a**). In all cases the solutions were 100 μM in the oligonucleotide. The evolution of the reactions was monitored by reversed-phase HPLC on Kromasil C_{18} columns (250 x 4.6 mm, 10 μm , flow rate: 1 mL/min), using linear gradients of aqueous triethylammonium acetate (0.05 M) (solvent A) and ACN (solvent B) or ACN/ H_2O 1:1 (solvent B'). Metal adducts were isolated after several HPLC runs by using analytical separation conditions. HR MALDI-TOF MS analysis was carried out in the negative mode using 2,4,6-trihydroxyacetophenone matrix with ammonium citrate as an additive.

1 Enzymatic digestions with 5'- and 3'-exonucleases (bovine spleen and snake venom phosphodiesterases,
2 respectively) were performed as previously described.^{41,42,43}
3
4

5 *Adduct* ^{5'}*dCATGGCT-conjugate 3*: R_t= 11.0 min (gradient: 15 to 50% B in 30 min); HR MALDI-TOF
6 MS, negative mode: *m/z* 3501.0 (calcd mass for C₁₂₈H₁₇₁N₃₈O₅₅P₆Pt [M-3H]⁻: 3500.95). MALDI-TOF
7 MS after digestion with snake venom phosphodiesterase: *m/z* 2907.9 (-pCpT) (calcd mass for
8 C₁₀₉H₁₄₆N₃₃O₄₂P₄Pt [M-3H]⁻: 2907.89). MALDI-TOF MS after digestion with bovine spleen
9 phosphodiesterase: *m/z* 2594.8 (-CpApTp) (calcd mass for C₉₉H₁₃₄N₂₈O₃₇P₃Pt [M-3H]⁻: 2594.83), *m/z*
10 2898.9 (-CpAp) (calcd mass for C₁₀₉H₁₄₇N₃₀O₄₄P₄Pt [M-3H]⁻: 2898.88).
11
12

13 *Adduct* ^{5'}*dCATGGCT-conjugate 4*: R_t= 21.2 min (gradient: 5 to 90% B' in 30 min); HR MALDI-TOF
14 MS, negative mode: *m/z* 3715.8 (calcd mass for C₁₄₄H₁₇₈N₃₇O₅₇OsP₆ [M-2H]⁻: 3715.02). MALDI-TOF
15 MS after digestion with snake venom phosphodiesterase: *m/z* 2793.0 (-pGpCpT) (calcd mass for
16 C₁₁₅H₁₄₁N₂₇O₃₈OsP₃ [M-2H]⁻: 2792.88). MALDI-TOF MS after digestion with bovine spleen
17 phosphodiesterase: *m/z* 2808.9 (-CpApTp) (calcd mass for C₁₁₅H₁₄₁N₂₇O₃₉OsP₃ [M-2H]⁻: 2808.87), *m/z*
18 3113.9 (-CpAp) (calcd mass for C₁₂₅H₁₅₄N₂₉O₄₆OsP₄ [M-2H]⁻: 3112.92).
19
20

21 *Adduct* ^{5'}*dCATGGCT-conjugate 5a*: R_t= 20.5 min (gradient: 5 to 90% B' in 30 min); HR MALDI-TOF
22 MS, negative mode: *m/z* 3540.8 (calcd mass for C₁₃₈H₁₈₃N₃₈O₅₅P₆Ru [M-3H]⁻: 3540.02). MALDI-TOF
23 MS after digestion with snake venom phosphodiesterase: *m/z* 2617.6 (-pGpCpT) (calcd mass for
24 C₁₀₉H₁₄₆N₂₈O₃₆P₃Ru [M-3H]⁻: 2617.87). MALDI-TOF MS after digestion with bovine spleen
25 phosphodiesterase: *m/z* 2633.7 (-CpApTp) (calcd mass for C₁₀₉H₁₄₆N₂₈O₃₇P₃Ru [M-3H]⁻: 2633.87), *m/z*
26 2937.7 (-CpAp) (calcd mass for C₁₁₉H₁₅₉N₃₀O₄₄P₄Ru [M-3H]⁻: 2937.91).
27
28

29 **NMR spectroscopy.** The samples of the conjugates were prepared by dissolving the appropriate amount
30 of compound in 500 μL of H₂O/DMSO-*d*₆ 8:2 to give 0.8 mM solutions. NMR spectra were acquired on
31 Bruker Avance spectrometers operating at 600 or 800 MHz, and processed with Topspin software.
32 NOESY experiments were acquired with mixing times of 150 and 300 ms, and TOCSY spectra were
33 recorded with standard MLEV-17 spin-lock sequence, and 80-ms mixing time. Water suppression in
34 H₂O experiments was achieved by including a WATERGATE module in the pulse sequence prior to
35
36
37
38
39
40
41
42
43
44
45
46
47
48
49
50
51
52
53
54
55
56
57
58
59
60

1 acquisition. NMR experiments were carried out at temperatures ranging from 0 °C to 25 °C. The spectral
2 analysis program Sparky⁴⁴ was used for semiautomatic assignment of the NOESY cross-peaks and
3 quantitative evaluation of the NOE intensities. Sequential assignment of the peptide moiety was carried
4 out using standard ¹H NMR techniques.
5
6
7
8

9 **Structural modeling.** Molecular dynamics calculations were carried out with the program Sybyl X-1.3
10 (Tripos Inc). Ten initial models for each conjugate were built from the dicarba analogue of octreotide **2**
11 coordinates.²⁴ Metal complex coordinates were built from crystallographic structures of similar
12 compounds.^{36,45} Each of the initial structures was minimized and then submitted to 300 ps of molecular
13 dynamics simulations. Explicit solvent and periodic boundary conditions were included in the
14 calculations. The last 50 ps of each run was averaged and energy minimized. Backbone geometry of
15 those peptide residues that do not exhibit significant chemical shift variations was loosely constrained
16 by imposing dihedral angle restraints. Analysis of the representative structures was carried out with the
17 programs Sybyl and MOLMOL.⁴⁶
18
19
20
21
22
23
24
25
26
27
28
29
30

31 **Immunocytochemistry.** MCF-7 cells were seeded on fibronectin-coated coverslips and allowed to
32 attach overnight. Then, the cells were incubated at 37 °C with medium containing 50 μM of **13** during 1,
33 3 and 6 h, or with medium alone as control. After that, the cells were washed with cold PBS (Gibco
34 BRL) and fixed with 4% paraformaldehyde in PBS for 15 min at 4 °C. The cells nucleus were stained
35 with 2 μg/mL Hoescht 33258 (excitation/emission: 352 nm/461 nm) during 15 min. After washing twice
36 with cold PBS, the cells coverslips were mounted using a fluorescence mounting medium (Dako,
37 Carpinteria, CA, USA) and examined using a Leica TCS-SP5 multiphoton and high-velocity spectral
38 confocal microscope (Leica Microsystems, Nussloch, Germany).
39
40
41
42
43
44
45
46
47
48

49 **Internalization experiments with **13** and **14**.** The uptake efficiency of **13** and **14** by the cells was
50 quantified by flow cytometry. The cells were seeded onto 12-well plates and allowed to attach for 24 h.
51 Next, the cells were treated at 37 °C with 50 μM of either **13** or **14** during 1, 3 and 6 h. After rinsing the
52 cells three times with cold PBS, the cells were harvested by trypsinization and the fluorescence of the
53 cells, corresponding to the uptake of the Fluorescein-modified peptides, was analysed using a
54
55
56
57
58
59
60

1 FACSCalibur (Becton Dickinson Immunocytometry Systems, San Jose, CA) equipped with the
2 CellQuest™ software (Becton Dickinson). Fluorescence intensity was represented on a four orders of
3 magnitude log scale (1–10.000). 10000 cells were analysed in each experiment.
4
5

6
7 **Cytotoxicity assays.** The cytotoxicity of the conjugates and of the control complexes in MCF-7, DU-
8 145 and CHO cells was determined by the MTT assay. Aliquots of 4.000 DU-145 cells, 3.500 MCF-7 or
9 2.000 CHO cells, were seeded onto flat-bottomed 96-well plates. 24 h later, the cells were treated for 72
10 h with the compounds at concentrations ranging from 0 μ M to 250 μ M. After removal of the treatment,
11 the cells were washed with PBS and incubated for 3 additional hours with 100 μ L of fresh culture
12 medium together with 10 μ L of MTT (Sigma-Aldrich). The medium was discarded and DMSO (Sigma-
13 Aldrich) was added to each well to dissolve the purple formazan crystals. Plates were agitated at room
14 temperature for 10 minutes and the absorbance of each well was determined on a Multiscan Plate
15 Reader (ELX800, Biotek, Winooski, USA) at a wavelength of 570 nm. Three replicates were used in
16 each experiment. For each treatment, the cell viability was determined as a percentage of the control
17 untreated cells, by dividing the mean absorbance of each treatment by the mean absorbance of the
18 untreated cells. The concentration that reduces by 50% the cell viability (IC_{50}) was established for each
19 compound.
20
21
22
23
24
25
26
27
28
29
30
31
32
33
34
35
36

37 **Ruthenium accumulation in cancer cells.** For ruthenium cellular uptake studies, 1.5×10^6 MCF-7 cells
38 were plated in 100 mm Petri dishes and allowed to attach for 48 h. Next, the plates were exposed to the
39 ruthenium-octreotide conjugate **6** or to the unconjugated ruthenium complex **17** at a concentration
40 corresponding to a fifth of their IC_{50} (12.5 μ M and 0.66 μ M, respectively). Additional plates were
41 incubated with medium alone as negative control. After 24 h of incubation, the cells were rinsed three
42 times with cold PBS and harvested by trypsinization. The number of cells in each sample was counted
43 manually in a haemocytometer using the trypan blue dye exclusion test. Then the cells were centrifuged
44 to obtain the whole cell pellet for ICP-MS analysis. All experiments were conducted in triplicate.
45
46
47
48
49
50
51
52
53
54
55

56 **ICP-MS analysis.** The whole cell pellets were dissolved in 300 μ L of concentrated 72 % v/v nitric acid,
57 and the samples were then transferred into wheaton v-vials (Sigma-Aldrich) and heated in an oven at
58
59
60

1 373 K for 18 h. The vials were then allowed to cool, and each cellular sample solution was transferred
2 into a volumetric tube and combined with washings with Milli-Q water (1.7 mL). Digested samples
3 were diluted 10 times with Milli-Q to obtain a final HNO₃ concentration of approximately 2.5% v/v.
4
5 Ruthenium content was analyzed on an ICP-MS Perkin Elmer Elan 6000 series machine at the Centres
6
7 Científics i Tecnològics of the Universitat de Barcelona. The solvent used for all ICP-MS experiments
8
9 was Milli-Q water with 1% HNO₃. The ruthenium standard (High-Purity Standards, 1000 µg/mL ± 5
10
11 µg/mL in 2% HCl) was diluted with Milli-Q water to 100 ppb. Ruthenium standards were freshly
12
13 prepared in Milli-Q water with 1% HNO₃ before each experiment. The concentrations used for the
14
15 calibration curve were in all cases 0, 1, 2, 5 and 10 ppb. The isotope detected was ¹⁰¹Ru and readings
16
17 were made in triplicate. Rhodium was added as an internal standard at a concentration of 10 ppb in all
18
19 samples.
20
21
22
23
24

25
26 **SSTR2 expression analysis.** SSTR2 expression on MCF-7, DU-145 and CHO cells surface was
27
28 determined by double immunofluorescence. The cells were first fixed with PBS-1.5% formaldehyde and
29
30 permeabilized with PBS-0.2% Tween 20 (Biorad). Then the cells were incubated with a monoclonal
31
32 antibody against human sst₂ receptor (R&D systems) during 30 min at 4 °C. After rinsing the cells with
33
34 PBS, the cells were incubated 30 min at 4 °C in the presence of the Alexa-Fluor 488-conjugated goat
35
36 anti-mouse IgG antibody (Invitrogen). Cells were washed again and the fluorescence was analyzed using
37
38 a flow cytometer (FACSCalibur, Becton Dickinson Immunocytometry Systems, San Jose, CA) equipped
39
40 with the CellQuest™ software (Becton Dickinson). The fluorescence intensity of the cells was
41
42 represented on a four orders of magnitude log scale (1–10.000). 10000 cells were analysed in each
43
44 experiment.
45
46
47
48

49
50 **Statistical analysis.** The statistical analysis was performed with the SPSS statistical software for
51
52 Windows (version 15.0; SPSS Inc., Chicago, IL, USA). Quantitative variables were expressed as mean
53
54 and standard error (SE). The normality of the data was tested using the Kolmogorov-Smirnov test. The
55
56 differences between data with normal distribution and homogeneous variances were analyzed using the
57
58 parametric Student's t test. A value of p<0.05 was considered significant.
59
60

1
2
3
4
5
6
7
8
9
10
11
12
13
14
15
16
17
18
19
20
21
22
23
24
25
26
27
28
29
30
31
32
33
34
35
36
37
38
39
40
41
42
43
44
45
46
47
48
49
50
51
52
53
54
55
56
57
58
59
60

RESULTS AND DISCUSSION

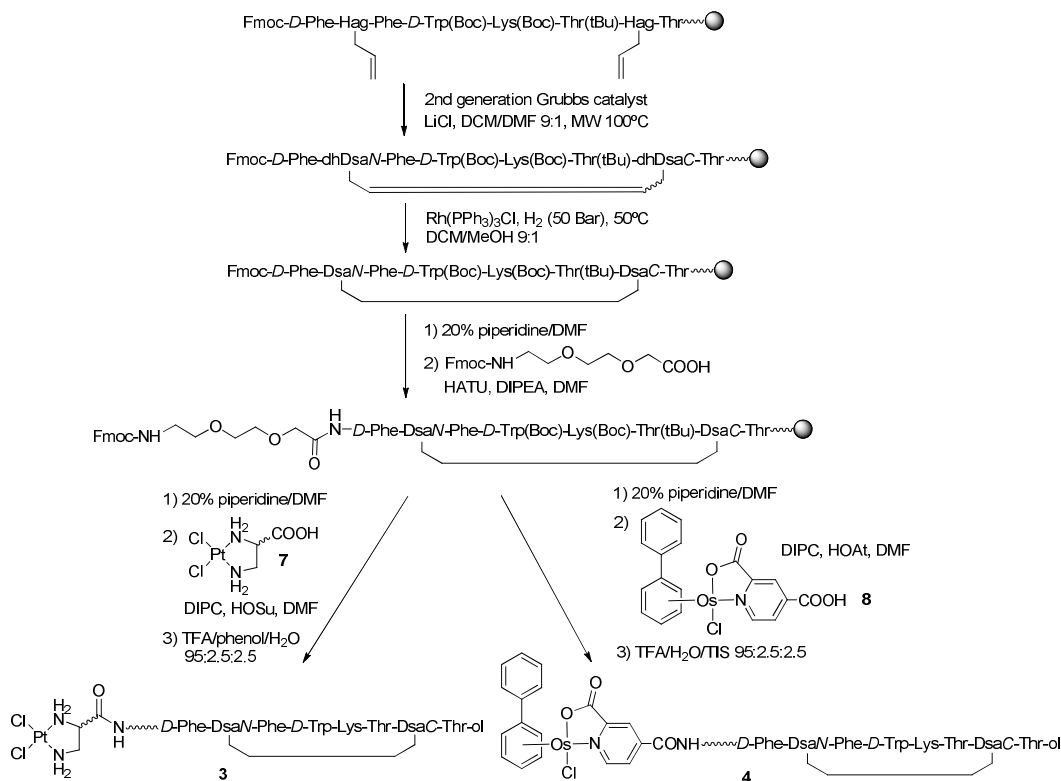
1
2
3
4
5
6
7
8
9
10
11
12
13
14
15
16
17
18
19
20
21
22
23
24
25
26
27
28
29
30
31
32
33
34
35
36
37
38
39
40
41
42
43
44
45
46
47
48
49
50
51
52
53
54
55
56
57
58
59
60

Synthesis and characterization of conjugates between a dicarba analogue of octreotide and dichloridoplatinum(II) and osmium(II) complexes. In our previous work,²³ *cis*-dichlorido-(1-(carboxylic acid)-1,2-diaminoethane)platinum(II) complex, ([PtCl₂(dap)]), was chosen as a cisplatin analogue since it can form the expected intrachain Pt-*N*7/5'*G*,*N*7/3'*G* chelates upon reaction with DNA. The attachment of the platinum complex to the γ -aminoisobutyryl-derivatized dicarba analogue of octreotide (**2**) was carried out on a solid-phase through the formation of an amide bond between its carboxylic function and the amine group of the spacer. Although the conjugate was able to bind to DNA in the same way as cisplatin, its low solubility in water precluded the evaluation of its biological activity. In order to improve the aqueous solubility for all the target conjugates, **3-6** (Chart 1), a polyethylenglycol spacer has been introduced between the peptide sequence and the metal complex. This spacer is expected to be sufficiently long to keep the metal complex away from the pharmacophore sequence.

Following our previous results on the synthesis of platinum(II)-octreotide conjugates, a stepwise solid-phase strategy has been used for the preparation of conjugates **3-6**. This approach is particularly useful in this case since it allows the regioselective introduction of the metal complex at the *N*-terminal end of the cyclic peptide. Otherwise, in a solution-phase approach the ϵ -NH₂ of the Lys residue would compete with the *N*-terminal amino group of octreotide. In order to increase the stability of the metal-octreotide conjugates, the CH₂-CH₂ linkage has been chosen as a disulfide isoster since this modification keeps a higher selectivity for sst₂ somatostatin receptor than the CH=CH linkage.²⁴

First, the linear peptide was synthesized manually on a Rink amide resin-*p*-MBHA using standard Fmoc-*t*Bu methodology (Scheme 1). All suitably-protected Fmoc-amino acids were incorporated with HATU in the presence of DIPEA in anhydrous DMF as a solvent. As previously described,^{23,24} Fmoc-protected threoninol functionalized as the *p*-carboxybenzaldehyde acetal was first anchored to the solid support. In addition, the two cysteine amino acids in octreotide were replaced by allyl glycine residues to perform the cyclization reaction. Once the linear peptide precursor had been assembled, on-resin

microwave-assisted ring closing metathesis was carried out with second-generation Grubbs catalyst for 1 h at 100 °C. Then, hydrogenation of the double bond using Wilkinson's catalyst afforded the protected cyclic saturated dicarba analogue of octreotide (**2**) bound to the resin. Finally, a Fmoc-protected polyethyleneglycol linker, 8-(9-fluorenylmethyloxycarbonyl-amino)-3,6-dioxaoctanoic acid, was incorporated at the *N*-terminal end using HATU as a coupling reagent.



Scheme 1. Schematic representation of the solid-phase approach used for the synthesis of conjugates **3** and **4**.

The final step involved the removal of the Fmoc protecting group of the spacer (20% piperidine in DMF) and the incorporation of the required metal complex onto the free amino function of the linker. For the synthesis of conjugate **3**, [PtCl₂(dap)] (**7**) was coupled using DIPC and NHS in anhydrous DMF (15 h at rt, protected from light).²³ Cleavage from the resin and removal of the protecting groups were carried out by treatment with a TFA/phenol/H₂O cocktail (95:2.5:2.5) for 1 h at rt. Reversed-phase HPLC analysis of the crude revealed a main double peak. Both peaks were isolated by semipreparative HPLC and characterized by HR MALDI-TOF and ESI MS and NMR as the expected diastereomeric

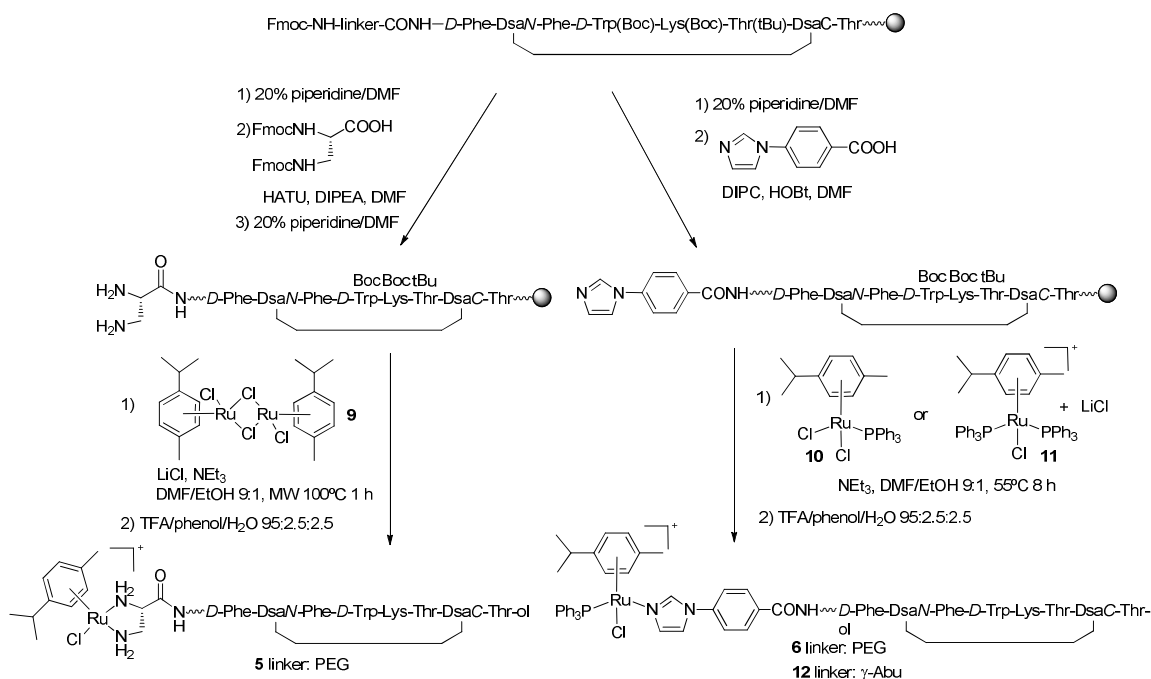
1 dichloridoplatinum(II)-octreotide conjugates, **3**. The generation of both isomers accounts from the use of
2 a racemic platinum(II) complex.
3

4 Our next objective was focused on the conjugation of an organometallic osmium(II) complex to the
5 dicarba analogue of octreotide. Among osmium complexes with anticancer activity, $[(\eta^6\text{-bip})\text{Os}(\text{pico})\text{Cl}]$
6 is particularly interesting since it exhibits promising activity in human ovarian cancer
7 cells.^{47,48} For this reason, we choose an analogue bearing a carboxylic function on the picolate ligand,
8 $[(\eta^6\text{-bip})\text{Os}(4\text{-CO}_2\text{-pico})\text{Cl}]$ (**8**), which would allow the attachment to octreotide. This complex has been
9 very recently conjugated to polyarginines with different chain lengths using solid-phase procedures.³⁰
10 Hence, for the synthesis of conjugate **4**, $[(\eta^6\text{-bip})\text{Os}(4\text{-CO}_2\text{-pico})\text{Cl}]$ was coupled either with PyBOP or
11 the more reactive HATU in the presence of DIPEA in anhydrous DMF (Scheme 1). After cleavage and
12 deprotection with a TFA/TIS/H₂O cocktail (95:2.5:2.5; 1 h at rt, protected from light), reversed-phase
13 HPLC analysis revealed a main peak (30-40%) which was isolated and characterized by HR MS and
14 NMR as the target conjugate **4**. The conversion yield was substantially increased (90%) when coupling
15 was performed with DIPC and HOAt in anhydrous DMF for 3 h. It is important to mention that during
16 HPLC analysis of conjugate **4**, a less retained peak was always observed, which was characterized by
17 MS as the aqua conjugate (substitution of Cl by H₂O). This result reveals fast hydrolysis kinetics for this
18 osmium(II) complex in comparison with that of the platinum(II) complex (see below).
19

20 **Synthesis and characterization of conjugates between a dicarba analogue of octreotide and**
21 **ruthenium(II) arene complexes.** Ruthenium-octreotide conjugates, **5** and **6**, were synthesized on a
22 solid-phase following a different strategy than that used for platinum and osmium conjugates (Scheme
23 2). Thus, instead of synthesizing the required ruthenium complexes bearing a carboxylic function, we
24 decided to incorporate the appropriate ligand at the *N*-terminal end of the linker-derivatized peptide,
25 which would allow the assembly of the organometallic ruthenium(II) complex around it. This approach
26 avoids some of the difficulties found during the synthesis of carboxylic acid-containing ruthenium
27 complexes and it could be applied to the parallel synthesis of libraries of ruthenium-peptide conjugates.
28
29
30
31
32
33
34
35
36
37
38
39
40
41
42
43
44
45
46
47
48
49
50
51
52
53
54
55
56
57
58
59
60

1 First, we focused on mononuclear ruthenium(II) arene complexes of the type $[(\eta^6\text{-arene})\text{RuCl}(\text{XY})]^+$,
2 where XY is a *N,N*-chelating ligand such as ethylenediamine. These compounds show high
3 cytotoxicities both *in vitro* and *in vivo*, with IC_{50} values comparable to carboplatin in human ovarian
4 cancer cell lines (e.g. 9 μM for $[(\eta^6\text{-}p\text{-cym})\text{RuCl}(\text{en})][\text{PF}_6]$).⁴⁹ In addition, they form monofunctional
5 adducts at guanine nucleobases on DNA.
6
7

8 Attachment of $[(\eta^6\text{-}p\text{-cym})\text{RuCl}(\text{en})]$ to octreotide was planned through the ethylenediamine ligand, as
9 performed for the dichloridoplatinum(II) conjugate, which would lead to conjugate **5** (Chart 1). In order
10 to incorporate 2,3-diaminopropionic acid into the *N*-terminal amino function of the linker-derivatized
11 dicarba analogue of octreotide bound to the resin, the required N^α, N^β -bis-(9-
12 fluorenylmethyloxycarbonyl)-*L*-2,3-diaminopropionic acid was synthesized by reaction between *L*-2,3-
13 diaminopropionic acid hydrochloride and 9-fluorenylmethyloxycarbonyl chloride. This Fmoc-protected
14 chelating ligand was coupled with HATU in DMF in the presence of DIPEA for 1 h at rt (Scheme 2).
15 After removal of the Fmoc protecting groups, the binding of the ruthenium arene to the chelating ligand
16 was studied by reaction with the ruthenium dimer $[\{(\eta^6\text{-}p\text{-cym})\text{Ru}(\mu\text{-Cl})\text{Cl}\}_2]$ (**9**). Optimized conditions
17 required microwave irradiation at 100 °C for 1 h and the use of a slight excess of **9** (3 mol equiv) in the
18 presence of LiCl (6.6 mol equiv) and NEt_3 (7.2 mol equiv) in a DCM/EtOH 9:1 mixture. The use of
19 microwave irradiation in combination with this solvent was proven to be particularly important to
20 achieve a good conversion yield. However, 30-40% conversion yields were obtained when DMF
21 replaced DCM and no irradiation was used (15 h heating at 60 °C). These results might be attributed to
22 the instability of **9** at high temperatures during a prolonged time. Cleavage from the resin and
23 deprotection was performed by treatment with a TFA/phenol/ H_2O cocktail (95:2.5:2.5) for 1 h at rt.
24 Reversed-phase HPLC analysis of the crude revealed a main peak (65%) which was isolated by
25 semipreparative HPLC and characterized by HR MALDI-TOF and ESI MS as the expected ruthenium-
26 octreotide conjugate, **5**.
27
28
29
30
31
32
33
34
35
36
37
38
39
40
41
42
43
44
45
46
47
48
49
50
51
52
53
54
55
56
57
58
59
60



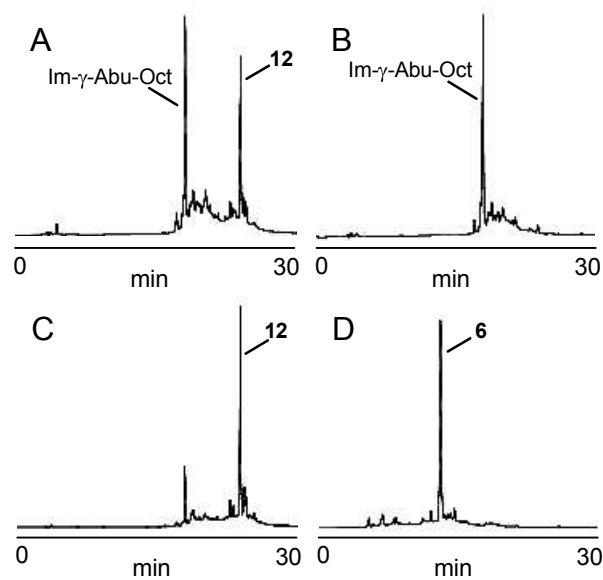
Scheme 2. Schematic representation of the solid-phase approach used for the synthesis of conjugates **5**, **6** and **12**.

Once we had synthesized conjugate **5**, we explored the possibility of assembling mononuclear ruthenium(II) arene complexes through a single monodentate ligand incorporated in the peptide fragment instead of using chelating ligands. On basis to the excellent antitumor activities of some ruthenium(II) three-legged “piano stool” complexes containing planar *N*-heteroaromatic sigma-bonded ligands and phosphine ligands,⁵⁰ with IC₅₀ values lower than that of cisplatin, we focused on compounds of the type $[(\eta^6\text{-}p\text{-cym})\text{RuCl}(\text{Im-Ph})(\text{PPh}_3)]^+$, where Im-Ph is 1-phenyl-imidazole. The conjugation of such triphenylphosphine-containing complexes to octreotide was planned through the phenyl ring linked to the imidazole ligand, which would allow the coordination of the ruthenium moiety. As in previous metal complexes, the hydrolysis of the Ru-Cl bond was expected to generate corresponding aqua species reactive towards DNA binding.

First, 4-(1*H*-Imidazol-1-yl)benzoic acid was coupled onto two batches of linker-octreotide resin with DIPC and HOBt in anhydrous DMF for 1 h at rt, where linker refers to γ -aminoisobutyryl group or the polyethylenglycol spacer (Scheme 2). The assembly of the metal complex was first explored with the γ -

1 Abu linker-containing batch by using two ruthenium compounds, $[(\eta^6\text{-}p\text{-cym})\text{RuCl}_2(\text{PPh}_3)]$ (**10**) and
2
3 $[(\eta^6\text{-}p\text{-cym})\text{RuCl}(\text{PPh}_3)_2]^+$ (**11**), since we hypothesized that the imidazole ligand could replace the more
4
5 labile chlorido ligands. **10** was easily synthesized by refluxing dimer **9** with triphenylphosphine (2.3 mol
6
7 equiv) in hexane for 15 h, whereas complex **11** was obtained from **10** by reaction with a slight excess of
8
9 triphenylphosphine (2 mol equiv) in methanol at 35 °C for 2.5 h.^{37,38}

12 Reaction of the imidazole-derivatized peptide-bound resin with complex **10** (4 mol equiv) was
13
14 performed in the presence of NEt_3 (16 mol equiv) in a DMF/EtOH mixture (3:1) for 8 h at 55 °C. After
15
16 treatment of the resin with a TFA/phenol/ H_2O cocktail (95:2.5:2.5), the desired conjugate **12** was
17
18 detected in the crude (18%) together with the imidazole-derivatized octreotide (20%), as inferred by
19
20 HPLC and MS analysis (Figure 1A).



23
24
25
26
27
28
29
30
31
32
33
34
35
36
37
38
39
40
41
42
43
44
45
46 **Figure 1.** Reversed-phase HPLC traces of the reaction crudes for the synthesis of conjugate **12** by using
47
48 complex **10** (A) or **11** (B) in the absence of LiCl or **11** in the presence of LiCl (C). Reaction crude for
49
50 the synthesis of conjugate **6** when **11** was used in the presence of LiCl (D).

1 We next investigated the reaction of octreotide-bound resin with complex **11** under the same conditions.
2
3 Unfortunately, reversed-HPLC analysis only revealed the presence of the imidazole-derivatized peptide,
4
5 which indicates that imidazole was not able to substitute the chloride ligand in **11** (Figure 1B). This
6
7 negative result might be attributed to the high steric hindrance around the metal because of the two
8
9 bulky PPh₃ ligands. However, to our surprise, when the reaction of **11** (4 mol equiv) with the peptide
10
11 was repeated in the presence of LiCl (4.4 mol equiv) and NEt₃ (16 mol equiv) in a DMF/EtOH 9:1
12
13 mixture for 8 h at 55 °C, HPLC analysis of the cleaved, deprotected crude (TFA/phenol/H₂O 95:2.5:2.5,
14
15 1 h rt) showed the presence of a main peak (57%) which was isolated and characterized by MS as
16
17 conjugate **12** (Figure 1C). Hence, imidazole is able to replace one of the two PPh₃ ligands in **11** instead
18
19 of the Cl ligand, thereby allowing the conversion yield of conjugate **12** to be improved in comparison
20
21 with that obtained when complex **10** is used. As shown in Figure 1D, the assembly of the ruthenium
22
23 complex by using these optimized conditions was almost quantitative onto the imidazole-derivatized
24
25 octreotide resin that contains the polyethyleneglycol linker, which allowed the target conjugate **6** to
26
27 obtain with high yield (Scheme 2). This compound was isolated by semipreparative HPLC and fully
28
29 characterized by HR MS and NMR.
30
31
32
33
34

35 In order to gain insight on the mechanism of this reaction, complex **11** was mixed with LiCl (1.4 mol
36
37 equiv) and NEt₃ (1.9 mol equiv) in anhydrous DMF and heated at 55 °C. As shown in the ³¹P NMR
38
39 spectra (Figure 2), the single chemical shift corresponding to the two PPh₃ ligands in **11** (δ: 20.0 ppm)
40
41 disappeared after 4 h. The two new signals (δ: 23.2 and -6.4 ppm) were assigned to the PPh₃ ligand in
42
43 complex **10** and to the released PPh₃, respectively. These results demonstrate the *in situ* generation of
44
45 complex **10** from **11** because of the presence of LiCl. This reaction might have future applications in the
46
47 synthesis of new ruthenium complexes for catalysis or biomedical applications.
48
49
50
51
52
53
54
55
56
57
58
59
60

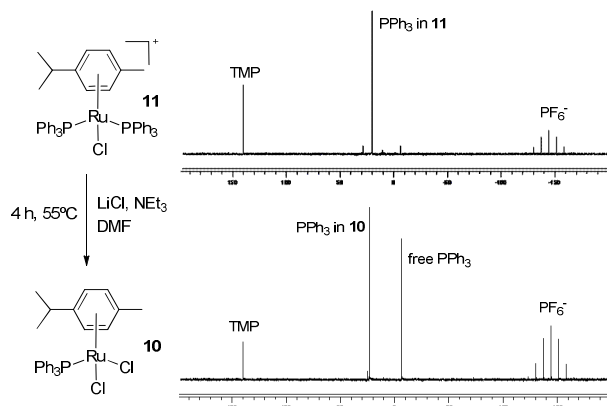


Figure 2. Schematic representation of the transformation of complex **11** to **10** (left) and ³¹P NMR spectra of **11** (A) and of the reaction crude after heating **11** in the presence of LiCl and NEt₃ for 4 h at 55 °C (B).

Activation of metal-octreotide conjugates by aqueous hydrolysis. In general, the cytotoxic activity of metal-based anticancer drugs is intimately related with the processes that mediate their activation in aqueous media; these processes are known to facilitate the interaction of the metal, its ligands or the complex or a fragment with the biological target (e.g. DNA, RNA or proteins). In addition, aqueous stability is another fundamental prerequisite since it might condition their success in clinical development. Cisplatin and its analogues can be considered prodrugs since their activation is produced through the dissociation of anionic ligands.^{22,51} The resulting positively charged aqua species coordinate strongly to nuclear DNA while neutral complexes do not, which demonstrates that in these family of compounds the metal plays a functional role.²² Organometallic complexes containing a labile group prone to substitution can also be activated inside the cells through hydrolysis. As previously stated, the activation of piano-stool organometallic ruthenium(II) complexes of the type $[(\eta^6\text{-arene})\text{RuCl}(\text{XY})]^+$, where XY is a neutral chelating ligand, proceeds through the release of chloride ligand. The resulting aqua species is responsible for ruthenation of DNA by generating monofunctional adducts on guanine nucleobases. In a similar manner to cisplatin and related platinum(II) compounds, the high extracellular chloride concentration (100 mM) in comparison with that present in the nucleus and cytoplasm (4 and 22.7 mM, respectively),⁵² ensures that the intact drug reaches its biological target before activation takes

1 place. In addition, a close correlation between cancer cell cytotoxic activity and the capacity of some
2 ruthenium(II) arene complexes to undergo hydrolysis of the Ru-halide bond has been established.⁵³
3
4 Osmium(II) arene complexes containing *N,N*-chelating ligands, such as ethylenediamine, experience
5
6 much slower ligand exchange kinetics than ruthenium analogues.⁵⁴ The higher acidity of the water
7
8 molecule bound to the osmium at physiological pH makes these compounds exist largely in their less
9
10 reactive hydroxido form. These problems have been solved by using picolinate as chelating ligand since
11
12 it increases both the hydrolysis rate and the basicity of the water molecule in the aqua species (e.g. [(η^6 -
13
14 arene)Os(pico)Cl]) and, for instance, generates compounds with similar anticancer activity as
15
16 ruthenium-arene analogues.^{36,47}
17
18
19
20
21

22 On the basis to these precedents, we wanted to assess whether hydrolysis of the M-Cl bond occurs when
23
24 Pt, Ru and Os complexes are conjugated to octreotide. The stability of conjugates **3-6** (Chart 1) was
25
26 investigated in aqueous solution at different chloride concentrations mimicking the typical of blood
27
28 plasma, cell cytoplasm and cell nucleus (100, 22.7 and 4 mM, respectively). In all cases, metal-
29
30 octreotide conjugates (10 μ M) were incubated at 37 °C for 24 h. In general, HPLC analysis showed that
31
32 the peak of the parent chloride compound (e.g. R_t = 20.3 min for conjugate **4**) evolved into a new less
33
34 retained peak (R_t =16.9 min), which was isolated and characterized by ESI MS as the aqua conjugate
35
36 (substitution of Cl by H₂O).
37
38
39

40
41 As previously found in some osmium(II) complexes,⁴⁸ the hydrolysis extent of conjugate **4** was highly
42
43 dependent on the NaCl concentration. Almost 95% of the conjugate was hydrolysed in the 4 mM NaCl
44
45 solution but the hydrolysis was substantially decreased in the more concentrated solutions of NaCl
46
47 (Table 1). These results indicate that the covalent attachment of the peptide does not interfere with the
48
49 hydrolysis properties of this osmium complex and,⁴⁸ more importantly, that the aqua species is not
50
51 deactivated by reaction with amino acids from the carrier peptide. Similar results were obtained for the
52
53 ruthenium conjugate **5** at the 4 mM chloride concentration. However, the extent of hydrolysis of the Ru-
54
55 Cl bond was substantially decreased at the higher NaCl concentrations (Table 1).
56
57
58
59
60

Regarding conjugate **3**, the hydrolysis of the Pt-Cl bond occurred to a lower extent than for conjugates **4** and **5** (only 16% after 24 h in 4 mM NaCl solution), and it was almost abolished at higher chloride concentration.

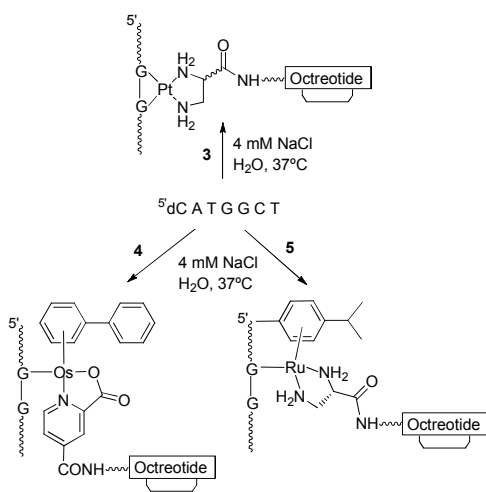
On basis to these results, it is expected that octreotide in conjugates **3** and **4** will have a positive effect on the delivery of the less reactive intact prodrug whilst outside the cell but, once in the cell cytoplasm and, particularly, in the cell nucleus, Pt and Os complexes will be selectively activated through hydrolysis to generate a species reactive towards DNA binding. However, hydrolysis of conjugate **5** in the blood plasma and in the cell cytoplasm might have important consequences for its biological activity since the metal complex could be deactivated by reaction with other potential ligands such as peptides or proteins.

To our surprise, no hydrolysis occurred in the case of conjugate **6** upon incubation for 24 h at 37 °C, as inferred by HPLC analysis together with MS (see below).

conjugate	% aqua adduct			% DNA adduct
	4 mM NaCl	22.7 mM NaCl	100 mM NaCl	4 mM NaCl
3	16	7	3	42
4	95	35	12	49
5a^a	97	83	74	37
6	0	0	0	0

Table 1. Percentage of aqua adduct formation in water at chloride levels typical of blood plasma (100 mM), cell cytoplasm (22.7 mM) and cell nucleus (4 mM), and percentage of the conjugate-DNA adduct formation in aqueous 4 mM NaCl. ^aSee the experimental section.

DNA binding studies. In general, the chlorido species of Pt(II), Ru(II) and Os(II) complexes are relatively less reactive towards DNA nucleobases in comparison with the aqua adducts. The chloride concentration in the nucleus of cells (ca. 4 mM) is much less than that in the cytoplasm (ca. 22.7 mM) or outside cells (ca. 100 mM) which favors the formation of reactive aqua adducts in the vicinity of DNA. We incubated conjugates **3-6** in 4 mM NaCl at 37 °C with the short DNA oligonucleotide, ^{5'}dCATGGCT. This oligonucleotide contains the target GG sequence of the anticancer drug cisplatin and is known to give the expected platinum 1,2-intrastrand GG chelates upon reaction either with cisplatin, [Pt(en)Cl₂] or a dichloridoplatinum(II) conjugate of a dicarba analogue of octreotide.^{23,41} In the case of the platinum conjugate **3**, HPLC analysis showed the formation of a new peak with higher retention time than the parent oligonucleotide (42% after 24 h; see Table 1), attributable to the hydrophobicity of the platinum-peptide fragment. This new product was isolated and characterized by HR MALDI-TOF MS as an adduct between **3** and ^{5'}dCATGGCT in which both chloride ligands had been lost. As expected from previous results,²³ MS analysis after enzymatic digestion with 5'- and 3'-exonucleases (bovine spleen and snake venom phosphodiesterases, respectively)^{42,43} revealed the formation of a chelate between the platinum fragment of the conjugate and both guanines of the DNA chain (Scheme 3).



Scheme 3. Formation of adducts between conjugates **3-5** and the oligonucleotide.

1 When osmium- and ruthenium(dap)-octreotide conjugates were incubated with $5'$ dCATGGCT, a major
2 monofunctional adduct was formed between the metal fragment of the conjugate and the DNA chain. In
3
4 both cases, the high metalation yield (49% for **4** and 37% for **5**) is in good agreement with the high
5
6 degree of hydrolysis of the Os/Ru-Cl bonds. Enzymatic digestion in combination with MS revealed that
7
8 in both cases metalation occurred at the guanine in the $5'$ position (G4, see Scheme 3). This is a similar
9
10 trend to that previously found with monofunctional platinum(II) complexes, such as $\{\text{Pt}(\text{dien})\}^{2+}$, since
11
12 they react exclusively with the $5'$ G nucleobase in the $5'$ dCATGGCT sequence.⁴¹ The high affinity of
13
14 similar ruthenium(II) arene complexes, such as $[(\eta^6\text{-}p\text{-cym})\text{RuCl}(\text{en})]^+$ or $[(\eta^6\text{-benzene})\text{Ru}(\text{en})(\text{OH}_2)]^{2+}$,
15
16 for the $N7$ position of guanine over the other DNA nucleobases has been observed previously.^{55,56,57}
17
18 Regarding organometallic osmium(II) complexes with picolinate ligands, such as $[(\eta^6\text{-}$
19
20 biphenyl) $\text{Os}(\text{picolinate})\text{Cl}]^+$, rapid binding to calf thymus DNA has also been found.⁵⁸
21
22 Finally, the reaction of the ruthenium-octreotide conjugate **6** with DNA was studied. In good agreement
23
24 with the absence of hydrolysis of the Ru-Cl bond in this compound, ruthenation of $5'$ dCATGGCT was
25
26 not observed even after 48 h.
27
28

29
30
31
32
33 The overall results demonstrate that the activation of the M-Cl bond through hydrolysis in the Ru and Os
34
35 conjugates seems to be very important for the binding to DNA, and that there is a strong preference for
36
37 the guanine nucleobases, especially those located at the $5'$ end in GG sequences. However, in the case of
38
39 the Pt(dap)-octreotide conjugate, platination is observed despite the slow kinetics for the hydrolysis of
40
41 the Pt-Cl bond in the low chloride medium as found in the nucleus. The high thermodynamic stability of
42
43 the $N7,N7$ -GG intrastrand adduct might account for this result.
44
45
46
47

48 **Efficiency of intracellular delivery of dicarba analogue of octreotide (2).** Compared to octreotide
49
50 (**1**), the binding affinity of the dicarba analogue of octreotide (**2**) (Chart 1) is slightly reduced for sst_2 ,
51
52 sst_4 and sst_5 receptors, although this reduction is smaller in the case of sst_2 receptor (about 23-fold for
53
54 sst_2 vs 36 and 48-fold for sst_4 and sst_5 , respectively).^{6,24} However, as previously stated, this high affinity
55
56 toward sst_2 receptor (44 nM) still makes **2** a suitable stabilized analogue of somatostatin to deliver
57
58
59
60

1
2
3
4
5
6
7
8
9
10
11
12
13
14
15
16
17
18
19
20
21
22
23
24
25
26
27
28
29
30
31
32
33
34
35
36
37
38
39
40
41
42
43
44
45
46
47
48
49
50
51
52
53
54
55
56
57
58
59
60

cytotoxic metal complexes into cancer cells. In order to check the capacity of internalization of analogue **2** in our cell lines by confocal microscopy and flow cytometry, we labelled it with fluorescein. For the synthesis of the fluorescein-labelled dicarba analogue of octreotide (**13**), 5(6)-carboxyfluorescein was coupled on the linker derivatized peptide-bound resin by using DIPC and HOAt as coupling reagents. Washings with 20% piperidine/DMF before the final acidic treatment yielded a highly pure peptide.⁵⁹ As a control, fluorescein-labelled octreotide (**14**) was also synthesized using solid-phase procedures.

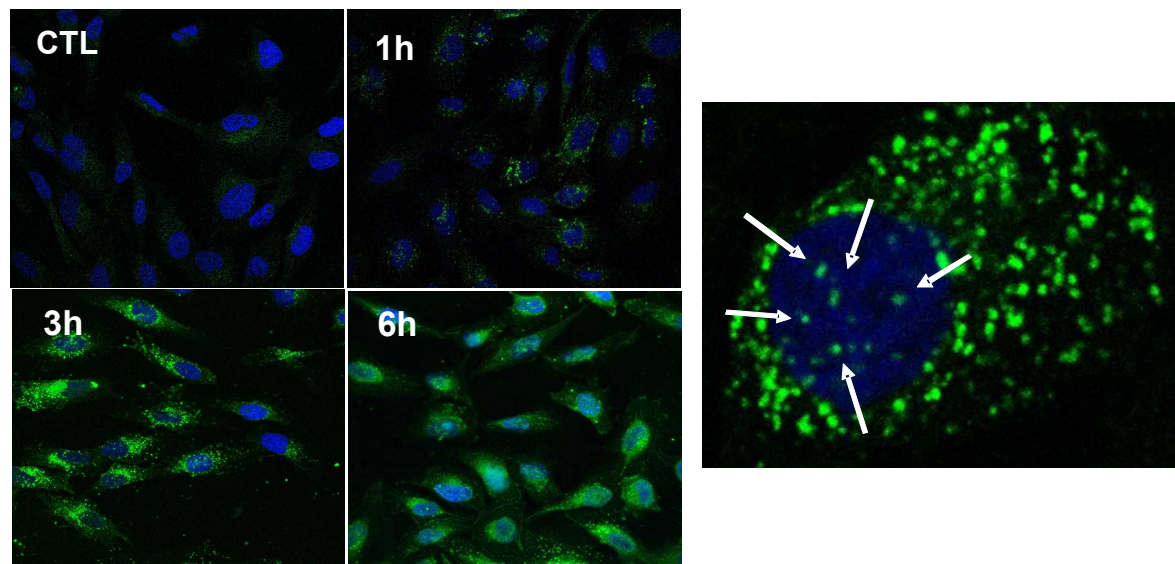


Figure 3. Confocal microscopic imaging of the internalization of the fluorescein-labelled dicarba analogue of octreotide (**13**) in MCF-7 cells. Left: MCF-7 cells incubated with 50 μM of **13** for 1, 3 and 6 h at 37 $^{\circ}\text{C}$ or medium alone as a control (CTL). The cell nuclei were stained with Hoechst (blue). The localization of **13** is indicated by the green fluorescence. Right: Higher magnification image (1000 x) of a MCF-7 cell incubated with 50 μM of **13** for 3 h at 37 $^{\circ}\text{C}$. Arrows indicate the nuclear localization of **13**.

Next, the internalization capacity of analogue **2** was determined by confocal microscopy, after the incubation of *sstr*₂-expressing human breast cancer MCF-7 cells with 50 μM of the corresponding fluorescein-labelled peptide (**13**) for different times (1, 3 and 6 h). After 1 h of treatment, fluorescent vesicles, most likely endosomes, were visible in the cytoplasm of most of the examined cells,

1 confirming the cellular uptake of the peptide (Figure 3). After 3 h and 6 h, the number and the
2 fluorescence density of the vesicles markedly increased, revealing an intense internalization of **13** during
3 this period of time. At these time points, the vesicles were mainly clustered at the periphery of the cell
4 nucleus. Higher magnification (1000x) images from cells exposed to **13** for 3 h (Figure 3) revealed that
5 although the fluorescence vesicles were located mainly in the cell cytoplasm, a small proportion of the
6 fluorescence was localized within the cell nucleus. Some authors have reported that somatostatin ligands
7 may accumulate in the cell nucleus,^{60,61} although the pathway for their nuclear localization remains to be
8 elucidated.
9

10 The qualitative observations in confocal microscopy studies were confirmed with quantitative data
11 obtained by flow cytometry. As represented in Figure 4A, the mean intracellular fluorescence intensity,
12 corresponding to the internalization of **13**, increased over time. The intracellular fluorescence intensity
13 increased from 78 ± 16 at 1 h to 111 ± 17 at 3 h and 182 ± 39 at 6 h confirming an active cellular uptake
14 of the peptide at these time points. In order to evaluate if **13** internalizes to a similar extent as native
15 octreotide, MCF-7 cells were incubated in parallel with **14**. As expected from the higher affinity of
16 octreotide for the somatostatin receptors,^{6,24} the intracellular uptake of **14** was more elevated, by 40-
17 57%, compared with that obtained in cells incubated with **13**. As shown in Figure 4B, the internalization
18 kinetics was parallel for both peptides and it is also in good agreement with previous reports.^{62,63}
19 Despite the differences in the amount of internalized peptide, these results demonstrate that the dicarba
20 analogue of octreotide (**2**) displays the internalization properties required to deliver the cytotoxic metal
21 complexes into cancer cells.
22
23
24
25
26
27
28
29
30
31
32
33
34
35
36
37
38
39
40
41
42
43
44
45
46
47
48
49
50
51
52
53
54
55
56
57
58
59
60

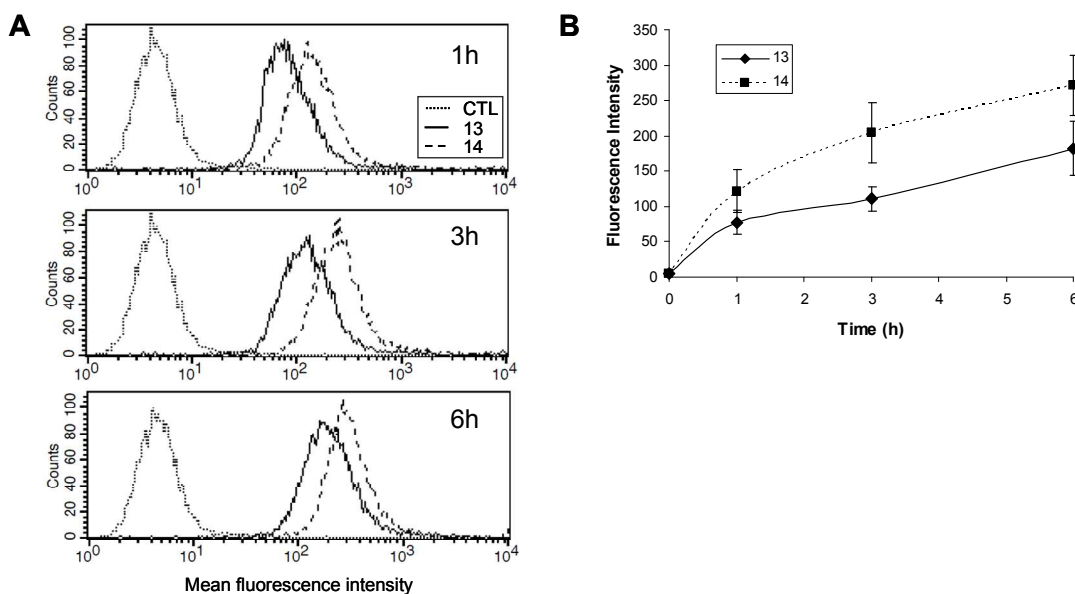


Figure 4. Intracellular delivery efficiencies of fluorescein-labelled dicarba analogue of octreotide (**13**) and of fluorescein-labelled octreotide (**14**) in MCF-7 cells. MCF-7 cells were incubated with the peptides for 1 h, 3 h and 6 h at 37 °C or medium alone (CTL). The fluorescence intensity of the cells, corresponding to the intracellular uptake of the peptides, was determined by flow cytometry. A: Flow cytometry histograms representing the fluorescence intensity of 10,000 cells on a four-decade log scale. Peptides **13** and **14** are depicted by solid and dashed lines, respectively. B: Kinetics of the cellular uptake of **13** and **14**. Each point in the graphs represents the mean intracellular fluorescence intensity of three independent experiments \pm SE.

Cancer Cell Cytotoxicity. To estimate the *in vitro* antitumor potential of the conjugates **3**, **4**, **5** and **6**, their antiproliferative activity was determined in the MCF-7 cell line. The compounds were screened at a wide range of concentrations (from 0 to 250 μ M) to determine the concentration that inhibits the cell growth by 50% (IC₅₀). The conjugates that did not inhibit cell growth by more than 50% at 250 μ M were considered to be inactive. As shown in Table 2, only conjugate **6** displayed a measureable antiproliferative activity, and even that was only moderate (IC₅₀ = 63.00 \pm 1.53). On basis to these results, we wondered whether the cytotoxic activity might be a consequence of the metal complex itself or of the conjugation to the peptide moiety. Hence, we tested the cytotoxicity of the parent metal

complex alone, including the ligand attached to the peptide. The following complexes were synthesized and used as controls (Chart 2): $[\text{PtCl}_2(\text{Etdap})]$ (**15**), $[(\eta^6\text{-}p\text{-cym})\text{RuCl}(\text{dap})]^+$ (**16**) and $[(\eta^6\text{-}p\text{-cym})\text{RuCl}(\text{Im-BzCOOMe})(\text{PPh}_3)]^+$ (**17**). Although we planned to mask the carboxylic function in all the complexes as a methyl or ethyl ester to avoid a negative charge that might hinder cell uptake and lower their biological activity, the complex $[(\eta^6\text{-}p\text{-cym})\text{RuCl}(\text{Etdap})]^+$ spontaneously hydrolysed to **16** during the work up of the reaction. Regarding the osmium complex $[(\eta^6\text{-bip})\text{OsCl}(4\text{-CO}_2\text{Et-pico})\text{Cl}]^+$ (**18**), a moderate cytotoxic activity in the human ovarian A2780 and A2780cis cell lines (IC_{50} = 44 and 61 μM , respectively) has been recently reported in comparison with that of $[(\eta^6\text{-bip})\text{OsCl}(4\text{-Me-pico})\text{Cl}]^+$ (IC_{50} = 4.4 and 7.6 μM in the A2780 and A2780cis cell lines, respectively).³⁶ Cytotoxicity assays of the control complexes revealed that **17** was highly effective in MCF-7 cells, displaying an IC_{50} value (3.32 ± 0.54) comparable to that of cisplatin in this cell line (IC_{50} = 3.04 ± 0.25). In contrast, a moderate antiproliferative activity was obtained for complex **15** (IC_{50} = 67.00 ± 19.01) while complex **16** was non-cytotoxic (Table 2).

	IC_{50} (μM)			
Conjugates	3	4	5	6
	> 250	> 250	> 250	63.00 ± 1.53
Complexes	15	-	16	17
	67.00 ± 19.01	-	> 250	3.32 ± 0.54

Table 2. IC_{50} values of conjugates **3-6** and control complexes **15-17** in MCF-7 cells. IC_{50} : Inhibitory concentration that reduce by 50% the cell viability. The cytotoxicity was determined by the MTT assay after 72 h of drug exposure. Data represents the mean \pm SE of at least three independent experiments.

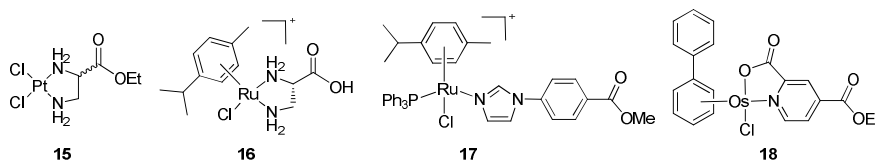


Chart 2. Structure of the control metal complexes.

Two important conclusions can be drawn from these results. First, a high cytotoxic activity of the metal complex itself seems to be crucial for the efficacy of the conjugates as antitumoral agents. Second, conjugation of the complexes to the peptide moiety diminishes their cytotoxic capacity. For example, the cytotoxic activity of the ruthenium(II) arene complex $[(\eta^6\text{-}p\text{-cym})\text{RuCl}(\text{Im-BzCOOMe})(\text{PPh}_3)]^+$ (**17**) is reduced about 19-fold when conjugated to the octreotide analogue (**6**), whereas complexes with moderate activity such as $[\text{PtCl}_2(\text{Etdap})]$ (**15**) or $[(\eta^6\text{-bip})\text{OsCl}(4\text{-CO}_2\text{Et-pico})\text{Cl}]^+$ (**16**),³⁶ afford inactive peptide conjugates (**3** and **4**, respectively). On the other hand, the lack of activity for complex $[(\eta^6\text{-}p\text{-cym})\text{RuCl}(\text{dap})]^+$ (**16**) or its octreotide conjugate (**5**) might be attributable to the high hydrolysis rate of the Ru-Cl bond, which would cause deactivation of the activated species by reaction with other biomolecules before it reaches nuclear DNA.

It is also interesting that the only conjugate that displays cytotoxic activity (**6**) does not interact with DNA, which can be attributed to the absence of hydrolysis of the Ru-Cl bond, even at a low chloride concentration (4 mM). This is also consistent with the fact that control complex **17** does not interact with double-stranded plasmid DNA after 48 h of incubation, as determined by electrophoretic mobility experiments (see Figure S-18 in the Supplementary Material). Similarly to conjugate **6**, the aqua adduct of complex **17** was only formed after overnight incubation with a large excess of AgNO_3 , as inferred by ^1H and ^{31}P NMR (see the Supplementary Material). The overall results suggest that the cytotoxic activity of **6** and **17** might not be a consequence of their coordination to *N*-donor ligands from nucleic acids (DNA or RNA) or proteins. However, it cannot be rule out that their activation under physiological conditions occurs through coordination to sulfur-containing amino acids in peptides such as glutathione or in proteins.

1 In order to gain insight into the implication of somatostatin subtype 2 receptor on the cytotoxic activity
2 of the ruthenium-octreotide conjugate **6**, the cellular uptake of this compound was compared with that of
3 of the unconjugated ruthenium complex **17**. Ruthenium accumulation (determined here as the net effect of
4 the unconjugated ruthenium complex **17**. Ruthenium accumulation (determined here as the net effect of
5 influx and efflux of Ru) in the MCF-7 cancer cell line was determined by ICP-MS after a 24 h exposure
6 to the compounds. Interestingly, the intracellular level of ruthenium after exposure to conjugate **6**
7 (143.14 ± 16.6 pmol Ru/10⁶ cells) was higher than that of the parent complex **17** (68.01 ± 2.2 pmol
8 Ru/10⁶ cells). Such a significant difference between these compounds reveals that conjugation to the
9 peptide moiety has a positive effect on the internalization of the ruthenium complex, thereby suggesting
10 that the attachment of the metal complex to the peptide does not disturb its active conformation and
11 hence its affinity toward somatostatin receptors is maintained (see below). Although the covalent
12 attachment of a potential metal-based drug to a receptor-binding peptide such as octreotide is expected
13 to increase the bioavailability, delivery and accumulation of the complex to cancer cells, it must also be
14 borne in mind that the peptide moiety might also inhibit or weaken the interaction of the metal fragment
15 with the final biological target (e.g., DNA, RNA, or proteins), which would compromise its cytotoxic
16 activity.²⁵ Release of the ruthenium fragment from the conjugate might be necessary to allow it to reach
17 its target site. This might explain the apparently contradictory results from cytotoxicity and cellular
18 uptake studies, since in this case the covalent attachment of the ruthenium complex to the dicarba
19 analogue of octreotide **2** increases uptake and accumulation of the drug in the cancer cell whilst the
20 cytotoxic activity of the final conjugate is reduced.

21
22
23
24
25
26
27
28
29
30
31
32
33
34
35
36
37
38
39
40
41
42
43
44
45
46 **Conformational analysis by NMR spectroscopy.** It is well-known from NMR studies in water and in
47 DMSO-*d*₆ solution that octreotide (**1**) adopts a predominant type II' β-turn conformation across residues
48 Phe⁷-*D*-Trp⁸-Lys⁹-Thr¹⁰.^{64,65} The stability of this conformation together with the orientation of exocyclic
49 residues (*D*-Phe² and Thr-ol¹⁵) plays an important role in the binding of octreotide and its analogues to
50 somatostatin receptors.^{66,67} Regarding the dicarba analogue of octreotide used in this work (**2**),
51 D'Addona et al. have recently described that replacement of cystine by a CH₂-CH₂ linkage does not
52
53
54
55
56
57
58
59
60

1 substantially alter the secondary structure in the active region.²⁴ These NMR studies also suggest that
2 there exists a conformational equilibrium between the antiparallel β -sheet structural cluster and a second
3 conformational ensemble involving folded structures for the *C*-terminal residues. This hypothesis is in
4
5 conformational ensemble involving folded structures for the *C*-terminal residues. This hypothesis is in
6
7 good agreement with previously reported findings for **1** that indicate that *C*-terminal amino acids fold
8
9 into a 3_{10} -helix-like array or in a similar helical ensemble.⁶⁶ Furthermore, it is important to consider that
10
11 the structure of **2** in the region of the *N*-terminal *D*-Phe² and *C*-terminal Thr(ol)¹⁵ is significantly
12
13 different from that previously reported for **1**,⁶⁶ which might explain the differences in affinity for
14
15 somatostatin receptors.²⁴ Given the implication of these amino acids both in the affinity and in the
16
17 specificity for somatostatin receptors, we investigated whether the covalent attachment of metal
18
19 complexes to the *N*-terminal end of **2** through a polyethylenglycol linker might alter the active
20
21 conformation of the peptide and, in particular, the structure around *D*-Phe² and Thr-ol¹⁵.
22
23
24
25
26

27 In order to gain some insight into peptide conformation, conjugates **3**, **4** and **6** were studied by 1D and
28
29 2D ¹H NMR spectroscopy. In all conjugates, significant line-broadening was observed at conjugate
30
31 concentrations above 1 mM, suggesting that oligomerization takes place under these conditions. This
32
33 effect is specially pronounced in the case of the osmium-octreotide conjugate (see the Supplementary
34
35 Material). To avoid oligomerization, 2D NMR spectra were recorded at a peptide concentration of 0.8
36
37 mM. Signals of the peptide were completely assigned using standard techniques (see Tables S1-3 in the
38
39 Supplementary Material). Resonances of the linker and of ligands in the metal fragments were also
40
41 identified, although not all of them could be unambiguously assigned to specific protons.
42
43
44
45

46 A comparison between the chemical shifts of the peptide fragment in the conjugates and the dicarba-
47
48 analogue of octreotide (**2**)²⁴ indicates that residues *D*-Trp⁸-Lys⁹-Thr¹⁰-DsaC¹⁴-Thr(ol)¹⁵ have very
49
50 similar chemical shifts, whereas significant differences are observed for protons of the amino acids *D*-
51
52 Phe²-DsaN³-Phe⁷ (Figure 5). This suggests that the peptide structure is only affected in the latter region.
53
54
55 The chemical shift of H α of *D*-Phe² is notably shifted downfield. This shift is attributed to the covalent
56
57 attachment of the linker to the α -amino group of this amino acid through an amide bond. Interestingly,
58
59
60

peaks for the NH protons of DsaN³ and Phe⁷ amino acids in all conjugates (and to a lesser extent for the H β signals) were shifted upfield.

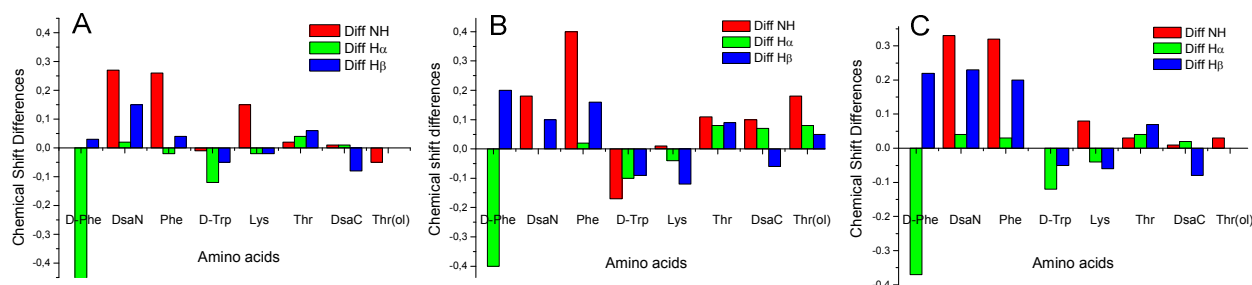
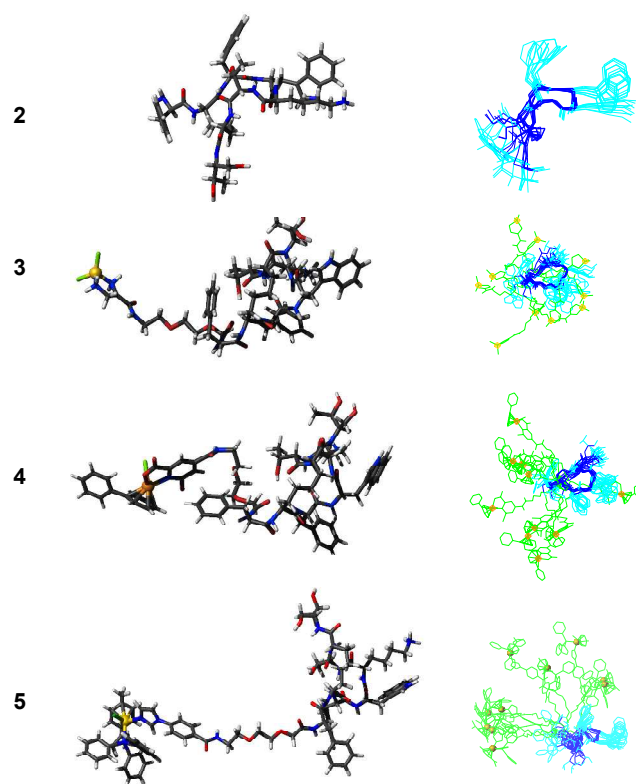


Figure 5. Chemical shift differences for NH, H α and H β protons between conjugates **3** (A), **4** (B) and **6** (C) and the dicarba analogue of octreotide (**2**).²⁴

Molecular dynamics calculations were carried out to gain further insight in the structural alterations induced in the peptide structure by the covalent attachment of the metal complex. The results are illustrated in Figure 6. The peptide backbone is not significantly altered with respect to the structure of the dicarba analogue of octreotide (**2**). In particular, the β -turn backbone geometry around residues *D*-Trp⁸-Lys⁹-Thr¹⁰-DsaC¹⁴-Thr(ol)¹⁵ is totally preserved. The main changes occur in residues *D*-Phe² and DsaN³. Side chain conformations are less defined than in **2**. Linker and ligand fragments are mainly disordered. In some of the calculated conformers the ligand or the linker exhibit contacts with aromatic residues *D*-Phe² and Phe⁷ as well as with DsaN³ (see Figure 6). These residues correspond to those that have changes in their ¹H NMR chemical shifts with respect to the unmodified peptide. This is also in good agreement with the fact that some NOEs were observed between the linker and *D*-Phe² (see Figure S-20 in the Supplementary Material).

The NMR data and molecular dynamics calculations suggest that the covalent attachment of the metal complex does not substantially alter the global structure of the peptide. However, the aromatic ligands of the ruthenium and osmium complex in conjugates **4** and **6** as well as the linker appear to have a

1 tendency to interact with the aromatic residues located to their near side of the peptide sequence, which
2 could be favoured by the high flexibility of the polyethyleneglycol linker. This is particularly important
3 in the case of the Phe⁷ residue, since this amino acid is included in the so-called pharmacophore
4 sequence of octreotide. These results support the hypothesis that the covalent attachment of both
5 fragments might generate a significant population of peptide conformations with a decreased affinity for
6 somatostatin receptors in comparison with that of the dicarba analogue of octreotide **2**. However, the
7 dicarba analogue of octreotide **2** still retains the ability to internalize metal complexes upon conjugation,
8 as demonstrated cellular uptake experiments with **6** and **17**.
9
10
11
12
13
14
15
16
17
18
19
20



21
22
23
24
25
26
27
28
29
30
31
32
33
34
35
36
37
38
39
40
41
42
43
44
45
46
47
48
49
50
51
52
53
54
55
56
57
58
59
60
Figure 6. Model structures of the dicarba analogue of octreotide (**2**) and of conjugates **3**, **4** and **6** (see Chart 1). Left: representative conformer. Right: ensemble with 10 conformers resulting from molecular dynamics calculations. Superposition was done by fitting the backbone peptide heavy atoms.

Selectivity of the ruthenium-octreotide conjugate (6). The main objective of a targeted strategy is the selective delivery of a cytotoxic drug to cancer cells in order to reduce toxicity to normal cells. Consequently, the reduction of the antiproliferative activity of a metal complex when conjugated with octreotide (Table 2) could be compensated by a selective and a more efficient delivery of the compound to the targeted cells. In order to corroborate this hypothesis, we determined whether the conjugation of the ruthenium(II) arene complex **17** to the octreotide analogue **2** (conjugate **6**) is correlated with its vehiculization to tumour cells overexpressing *sstr₂*, the most relevant receptor for octreotide internalization.⁶⁸ To this end, we further analyzed the cytotoxic activity of conjugate **6** in human prostate tumour DU-145 cells as well as and in the Chinese hamster ovary (CHO) cell line, in order to assess the selectivity of the ruthenium-octreotide conjugate for cancer cells with respect to normal cells (Table 3). As shown in Fig. 7A, DU-145 cells were markedly more responsive to **6** than the MCF-7 and CHO cells, as the IC₅₀ value (26.00 ± 3.46) was 2.4-fold lower than in MCF-7 cells and about 1.7-fold lower than in CHO cells (IC₅₀: 45.17 ± 2.61) (Table 3). This difference in the cytotoxic activity of conjugate **6** between the cell lines cannot be attributed to a different activity of the metal fragment in the different cells, as the control complex **17** cytotoxicity was higher in MCF-7 (IC₅₀= 3.32 ± 0.54) and more attenuated in DU-145 cells (IC₅₀= 6.80 ± 0.99) and CHO cells (5.8 ± 0.01) (Figure 7B) (Table 3).

Cell line, IC₅₀ (μM)

Compound	MCF-7	DU-145	CHO
6	63.00 ± 1.53	26.00 ± 2.00	45.17 ± 2.61
17	3.32 ± 0.54	6.80 ± 0.99	5.8 ± 0.01

Table 3. IC₅₀ values of the ruthenium-octreotide conjugate **6** and control complex **17** in human cancer cell lines (MCF-7 and DU-145) and in normal cells (CHO). IC₅₀: Inhibitory concentration that reduce by 50% the cell viability. The cytotoxicity was determined by the MTT assay after 72 h of drug exposure. Data represents the mean \pm SE of at least three independent experiments.

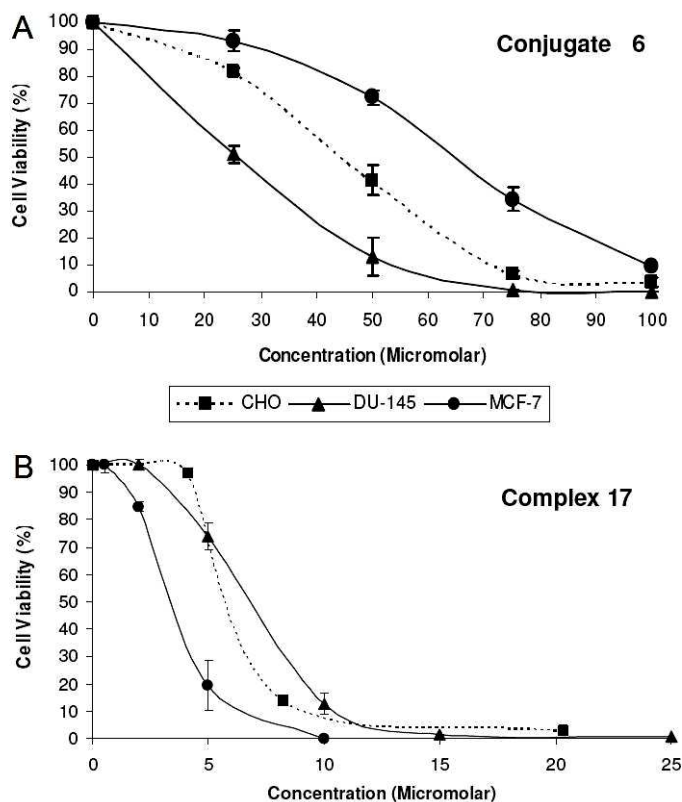


Figure 7. Cytotoxic effect of conjugate **6** (A) and complex **17** (B) in the MCF-7, DU-145 and CHO cell lines. Cells were treated for 72 h with the indicated concentrations of each compound. The cell viability was determined using the MTT assay. Each point in the graphs represents the mean of three independent experiments \pm SE.

In order to determine if the cytotoxic activity of **6** was related to the receptor expression on the cell surface, we next characterized the $sstr_2$ levels by flow cytometry. As shown in Figure 8A, $sstr_2$ expression was detected on the three cell lines. Notably, $sstr_2$ expression was significantly higher in the DU-145 and CHO cells than in MCF-7 cells (mean cell fluorescence intensity 347.5 ± 54.6 ; 344.0 ± 50.56 and 206.7 ± 14.27 , respectively) (Figure 8B), which demonstrates that the cytotoxic activity of **6** is strongly correlated with $sstr_2$ expression levels, specially in the DU-145 and MCF7 cells. However, although the CHO cells displayed similar $sstr_2$ expression levels than DU-145, the toxicity of **6** was attenuated in these cells, suggesting some selective cytotoxic activity of the ruthenium-octreotide conjugate towards cancer cells with respect to normal cells.

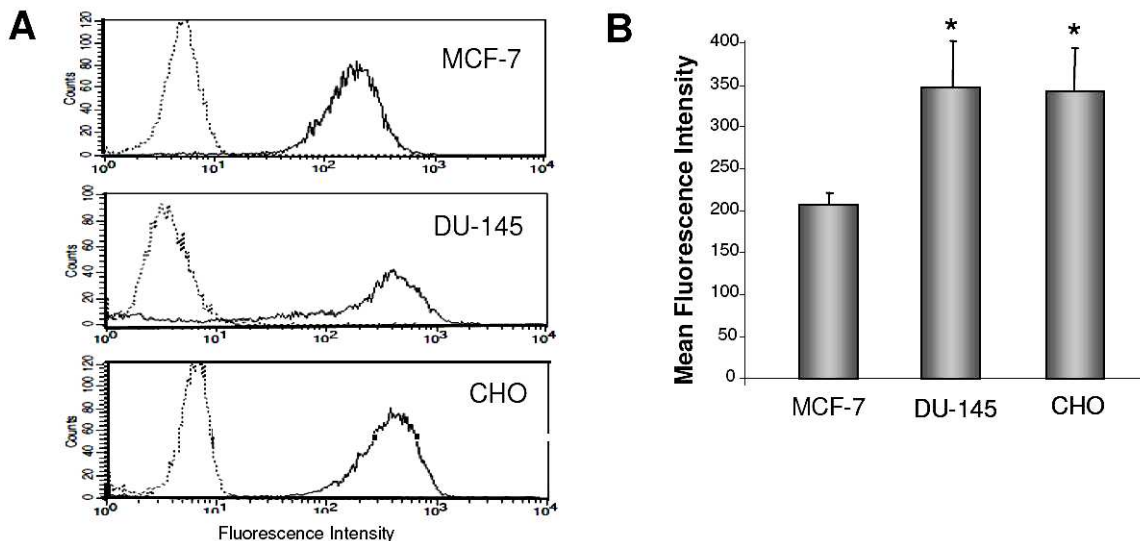


Figure 8. Expression of the ssr_2 receptor on MCF-7, DU-145 and CHO cell lines. A: Representative flow cytometry histograms obtained after the indirect immunofluorescence staining of the cells. Solid lines represent the fluorescence intensity of the cells after the incubation with an antibody against ssr_2 together with a control secondary antibody. Dotted lines indicate the background staining with the secondary antibody alone. B: Each column in the graphs represents the mean fluorescence intensity of three independent experiments \pm SE in MCF-7, DU-145 and CHO cells * $P < 0.05$ vs MCF-7 cells.

As a very weak expression of ssr_2 has been previously reported in CHO cells,⁶⁹ the ssr_2 expression in this cell line was additionally examined according to their mRNA expression levels. PCR analyses confirmed ssr_2 gene expression in CHO cells, with similar mRNA levels than in MCF-7 cells (see the Supplementary Material). Our results are in keeping with different studies describing that somatostatin receptors can also be identified in a broad panel of normal tissues, as well as in the human immune system.⁷⁰ As a consequence, new clinical applications for somatostatin analogues in several benign pathological diseases are emerging in addition to their role in malignant diseases.

1 All together, our results demonstrate a good correlation between the antitumour activity of the
2 ruthenium-octreotide conjugate **6** and the expression of the sst₂ receptor on the cell surface and reveal
3 the potential of conjugation with receptor-binding peptides such as octreotide to deliver metal-based
4 anticancer drugs specifically to cells overexpressing somatostatin subtype 2 receptor.
5
6
7
8
9
10
11
12
13
14
15
16
17
18
19
20
21
22
23
24
25
26
27
28
29
30
31
32
33
34
35
36
37
38
39
40
41
42
43
44
45
46
47
48
49
50
51
52
53
54
55
56
57
58
59
60

CONCLUSIONS

1
2
3 In summary, in this work we have described a straightforward solid-phase methodology for the
4 conjugation of a dichloridoplatinum(II) complex as well as three “piano-stool” organometallic
5 ruthenium(II) and osmium(II) complexes to a dicarba analogue of octreotide, a potent somatostatin
6 agonist whose receptors, particularly subtype 2, are overexpressed on the membrane of tumor cells. At
7 nuclear Cl⁻ concentration (4 mM), platinum (**3**), osmium (**4**) and Ru(dap) (**5**) conjugates are activated
8 through hydrolysis of the M-Cl, which correlates well with their DNA binding capacity, revealing in all
9 cases a strong preference for guanine nucleobases. However, neither hydrolysis of the Ru-Cl nor
10 interaction with DNA was observed in the case of the triphenylphosphine-containing ruthenium
11 conjugate (**6**). Surprisingly, the latter conjugate displays antiproliferative activity but the rest of
12 conjugates were non-cytotoxic. Additional cytotoxic experiments with control metal complexes and
13 cellular uptake experiments by ICP-MS, as well as conformational analysis of metal-octreotide
14 conjugates by 2D NMR spectroscopy and molecular dynamics calculations have allowed us to establish
15 three general conclusions. First, a significant loss in the cytotoxic activity of the metal complex moiety
16 always occurs when conjugated to the peptide sequence (e.g. IC₅₀=3.32 ± 0.54 in MCF-7 cells and
17 IC₅₀=6.80 ± 0.99 in DU-145 cells for complex **17** vs IC₅₀= 63.00 ± 1.53 in MCF-7 cells and IC₅₀= 26.00
18 ± 2.00 in DU-145 cells for conjugate **6**); hence, it seems to be important to use metal complexes with
19 high cytotoxic activity in order to develop peptide-conjugates with active biological properties. Second,
20 despite the presence of some altered amino acids in the pharmacophore sequence of octreotide,
21 particularly at the *N*-terminal end of the peptide, the overall structure is essentially maintained in the
22 conjugate, which suggests that the affinity for somatostatin receptors would not be compromised upon
23 conjugation to a metal complex; this observation is in good agreement with the higher accumulation of
24 ruthenium in cancer cells upon exposure to the ruthenium-octreotide conjugate **6** in comparison with
25 that of the parent complex **17**, which demonstrates that the peptide has a positive effect on the
26 internalization of the ruthenium complex. The choice of the spacer is also important, not only to
27
28
29
30
31
32
33
34
35
36
37
38
39
40
41
42
43
44
45
46
47
48
49
50
51
52
53
54
55
56
57
58
59
60

1 improve aqueous solubility and to keep the metal complex away from the peptide, but also to reduce
2 conformational freedom between both fragments in the conjugate. Third, the significantly higher
3 expression of the sst₂ receptor on DU-145 cells compared to MCF-7 cells is in good agreement with the
4 intracellular uptake of the fluorescein-labelled dicarba analogue of octreotide (**13**), since it is markedly
5 higher in the prostate tumour cells than in breast cancer cells. The fact that control complex **17** shows an
6 attenuated cytotoxicity in DU-145 cells compared with MCF-7 cells suggests that the antitumoral
7 activity of the ruthenium-octreotide conjugate **6** is correlated with the overexpression of the sst₂ receptor
8 on the cell surface. The cytotoxic activity of **6** in a non-tumour cell line (CHO) was similar to that found
9 in cancer cells, a result which can be attributed to a similar level of expression of somatostatin subtype-2
10 receptors.
11

12 The overall results of this work demonstrate the potential of conjugation between metal-based anticancer
13 drugs and receptor-binding peptides such as octreotide to target tumoral cells through binding to specific
14 receptors, including somatostatin subtype 2 receptor, overexpressed in their membranes. In the near
15 future, this receptor-targeted anticancer strategy is expected to generate new antitumor drugs with
16 reduced side-effects and reduced toxicity in normal cells. The potential of this strategy will be increased
17 by using novel approaches to circumvent some of the limitations found in this work, particularly new
18 biological vectors in combination with photoactivated metal complexes²⁵ or cleavable linkers³² in the
19 biological media. Work is in progress in this direction to generate more specific metal-based anticancer
20 drugs.
21
22
23
24
25
26
27
28
29
30
31
32
33
34
35
36
37
38
39
40
41
42
43
44
45
46
47
48
49
50
51
52
53
54
55
56
57
58
59
60

ACKNOWLEDGEMENTS

This work was supported by funding from the Ministerio de Educación y Ciencia (CTQ2005-01834, CTQ2007-68014, CTQ2008-02064 and CTQ2010-21567), the Generalitat de Catalunya (2009SGR208 and Xarxa de Referència de Biotecnologia), Instituto de Salud Carlos III (grants RD06/0020/0041), the Programa d'Intensificació de la Recerca (UB) and the ERC (grant no 247450, to PJS). We thank Prof. Alfonso Carotenuto (University of Napoli) for providing the coordinates of the dicarba analogue of octreotide **2**, Dr. Sabine H. van Rijt (University of Warwick) for supplying the osmium complex **8** and Dr. Isolda Romero (University of Warwick) and Dr Antoni Padró (Centres Científics i Tecnològics, Universitat de Barcelona) for helpful assistance in the determination of ruthenium content by ICP-MS.

ASSOCIATED CONTENT

Supporting Information: Selected MS spectra and HPLC traces of metal complex-octreotide conjugates and of DNA-conjugate adducts. NMR data of conjugates **3**, **4** and **6**, and of control metal complexes. sstr2 mRNA expression in CHO and MCF-7 cells. This material is available free of charge via the Internet at <http://pubs.acs.org>.

AUTHOR INFORMATION

Corresponding author: *(Vicente Marchán) Phone: +34 934021249, Fax: +34 933397878, E-mail: vmarchan@ub.edu; (Anna Massaguer) Phone: +34 972418370, Fax: +34 972418150, E-mail: anna.massaguer@udg.edu.

ABBREVIATIONS USED

Abu, aminoisobutyryl; ACN, acetonitrile; bip, biphenyl; cym, cymene (1-methyl-4-(1-methylethyl)benzene); dap, 1-(carboxylic acid)-1,2-diaminoethane; DCM, dichloromethane; dhDsaC, dehydrodiaminosuberic acid *C*-terminus; dhDsaN, dehydrodiaminosuberic acid *N*-terminus; DIPC, *N,N'*-diisopropylcarbodiimide; DIPEA, *N,N*-diisopropylethylamine; DMF, *N,N*-dimethylformamide; DMSO, dimethylsulfoxide; DTPA, diethylenetriamino-pentaacetic acid; DOTA, 1,4,7,10-

1 tetraazacyclododecane-1,4,7,10-tetraacetic acid; DsaC, diaminosuberic acid C-terminus; DsaN,
2 diaminosuberic acid N-terminus; ESI, electrospray ionization; Fluo, 5(6)-carboxyfluorescein; Fmoc, 9-
3 fluorenylmethyloxycarbonyl; Hag, L-2-allyl-glycine; HATU: hexafluorophosphate salt of the (2-(7-aza-
4 1H-benzotriazol-1-yl)-1,1,3,3-tetramethyluronium; HOAt, 1-hydroxy-7-azabenzotriazole; HOBt, 1-
5 hydroxybenzotriazole; HR-ESI, high-resolution electrospray ionization; ICP-MS, inductively coupled
6 plasma mass spectrometry; Im, imidazole; Ind, indazole; MALDI-TOF, matrix-assisted laser desorption
7 ionization time-of-flight; MS, mass spectrometry or mass spectrum; MTT, 3-(4,5-dimethylthiazol-2-yl)-
8 2,5-diphenyltetrazolium bromide; NHS, N-hydroxysuccinimide; NOE, nuclear Overhauser effect;
9 NOESY, nuclear Overhauser enhanced spectroscopy; PBS, Phosphate Buffered Saline; PEG,
10 polyethylenglycol; pico, picolinate; sst, somatostatin; sstr, somatostatin receptor; TIS, triisopropylsilane;
11 TMP, trimethylphosphite; TFA, trifluoroacetic acid.
12
13
14
15
16
17
18
19
20
21
22
23
24
25
26

27 REFERENCES

- 28
29
30 (1) Reubi, J. C. (2003) Peptide receptors as molecular targets for cancer diagnosis and therapy. *Endocr.*
31 *Rev.* 24, 389-427.
32
33
34
35 (2) Zaccaro, L., del Gatto, A., Pedone, C., and Saviano, M. (2009) Peptides for tumour therapy and
36 diagnosis: Current status and future directions. *Curr. Med. Chem.* 16, 780-795.
37
38
39 (3) Okarvi, S. M. (2008) A comprehensive overview of peptide-based radiopharmaceuticals and
40 cytotoxic conjugates, as well as their potential applications in cancer diagnosis and therapy. *Cancer*
41 *Treat. Rev.* 34, 13-26.
42
43
44 (4) Mezo, G., and Manea, M. (2010) Receptor-mediated tumor targeting based on peptide hormones.
45 *Expert. Opin. Drug. Deliv.* 7, 79-96.
46
47
48 (5) Schaer, J. C., Waser, B., Mengod, G., and Reubi, J. C. (1997) Somatostatin receptor subtype
49 expression in human pituitary, gastroentero-pancreatic and mammary tumors: comparison of mRNA
50 analysis with receptor autoradiography. *Int. J. Cancer* 70, 530-537.
51
52
53
54
55
56
57
58
59
60

- 1 (6) Janecka, A., Zubrzycka, M., and Janecki, T. (2001) Somatostatin analogs. *J. Pept. Res.* 58, 91-107.
- 2
- 3 (7) Bauer, W., Briner, U., Dopfener, W., Haller, R., Huguenin, R., Marbach, P., Petcher, T. J., and
- 4
- 5 Pless, J. (1982) SMS 201-995: a very potent and selective analogue of somatostatin with prolonged
- 6
- 7 action. *Life Sci.* 31, 1133-1140.
- 8
- 9
- 10
- 11 (8) de Jong, M., Breeman, W. A. P., Kwekkeboom, D. J., Valkema, R., and Krenning, E. P. (2009)
- 12
- 13 Tumor imaging and therapy using radiolabeled somatostatin analogues. *Acc. Chem. Res.* 42, 873-880.
- 14
- 15
- 16
- 17 (9) Sun, L.-C., and Coy, D. H. (2008) Cytotoxic conjugates of peptide hormones for cancer
- 18
- 19 chemotherapy. *Drugs Future* 33, 217-223.
- 20
- 21
- 22
- 23 (10) Wheate, N. J., Walker, S., Craig, G. E., and Oun, R. (2010) The status of platinum anticancer
- 24
- 25 drugs in the clinic and in clinical trials. *Dalton Trans.* 39, 8113-8127.
- 26
- 27
- 28 (11) Jakupec, M. A., Galanski, M., Arion, V. B., Hartinger, C. G., and Keppler, B. K. (2008)
- 29
- 30 Antitumour metal compounds: more than theme and variations. *Dalton Trans.* 183-194.
- 31
- 32
- 33
- 34 (12) van Rijt, S. H., and Sadler, P. J. (2009) Current applications and future potential for bioinorganic
- 35
- 36 chemistry in the development of anticancer drugs. *Drug Discov. Today* 14, 1089-1097.
- 37
- 38
- 39 (13) Rademaker-Lakhai, J. M., Van den Bongard, D., Pluim, D., Beijnen, J. H., and Schellens, J. H. M.
- 40
- 41 (2004) A phase I and pharmacological study with imidazolium-*trans*-DMSO-imidazole-
- 42
- 43 tetrachlororuthenate, a novel ruthenium anticancer agent. *Clin. Cancer Res.* 10, 3717-3727.
- 44
- 45
- 46
- 47 (14) Jakupec, M. A., Arion, V. B., Kapitza, S., Reisner, E., Eichinger, A., Pongratz, M., Marian, B.,
- 48
- 49 Graf von Keyserlingk, N., and Keppler, B. K. (2005) KP1019 (FFC14A) from bench to bedside:
- 50
- 51 preclinical and early clinical development - an overview. *Int. J. Clin. Pharmacol. Ther.* 43, 595-596.
- 52
- 53
- 54
- 55 (15) Peacock, A. F. A., and Sadler, P. J. (2008) Medicinal organometallic chemistry: Designing metal
- 56
- 57 arene complexes as anticancer agents. *Chem. Asian J.* 3, 1890-1899.
- 58
- 59
- 60

- 1
2
3
4
5
6
7
8
9
10
11
12
13
14
15
16
17
18
19
20
21
22
23
24
25
26
27
28
29
30
31
32
33
34
35
36
37
38
39
40
41
42
43
44
45
46
47
48
49
50
51
52
53
54
55
56
57
58
59
60
- (16) Levina, A., Mitra, A., and Lay, P. A. (2009) Recent developments in ruthenium anticancer drugs. *Metallomics 1*, 458-470
- (17) Casini, A., Hartinger, C. G., Nazarov, A., and Dyson, P. J. (2010) Organometallic antitumour agents with alternative modes of action. *Top. Organomet. Chem. 32*, 57-80
- (18) Gasser, G., Ott, I., and Metzler-Nolte, N. (2011) Organometallic anticancer compounds. *J. Med. Chem. 54*, 3-25.
- (19) Süss-Fink, G. (2010) Arene ruthenium complexes as anticancer agents. *Dalton Trans. 39*, 1673-1688.
- (20) Wang, F., Chen, H., Parsons, S., Oswald, I. D. H., Davidson, J. E., and Sadler, P. J. (2003) Kinetics of aquation and anation of ruthenium(II) arene anticancer complexes, acidity and X-ray structures of aqua adducts. *Chem. Eur. J. 9*, 5810-5820.
- (21) Kostrhunova, H., Florian, J., Novakova, O., Peacock, A. F. A., Sadler, P. J., and Brabec, V. (2008) DNA interactions of monofunctional organometallic osmium(II) antitumor complexes in cell-free media. *J. Med. Chem. 51*, 3635-3643
- (22) Pizarro, A. M., Habtemariam, A., and Sadler, P. J. (2010) Activation mechanisms for organometallic anticancer complexes. *Top. Organomet. Chem. 32*, 21-56.
- (23) Barragán, F., Moreno, V., and Marchán, V. (2009) Solid-phase synthesis and DNA binding studies of dichloroplatinum(II) conjugates of dicarba analogues of octreotide as new anticancer drugs. *Chem. Commun.* 4705-4707.
- (24) D'Addona, D., Carotenuto, A., Novellino, E., Piccand, V., Reubi, J. C., Di Cianni, A., Gori, F., Papini, A. M., and Ginanneschi, M. (2008) Novel sst5-selective somatostatin dicarba-analogs: Synthesis and conformation-affinity relationships. *J. Med. Chem. 51*, 512-520.

1 (25) Barragán, F., López-Senín, P., Salassa, S., Betanzos-Lara, S., Habtemariam, A., Moreno, V.,
2 Sadler, P. J., and Marchán, V. (2011) Photocontrolled DNA binding of a receptor-targeted
3 organometallic ruthenium(II) complex. *J. Am. Chem. Soc.* 133, 14098–14108.
4

5
6
7
8 (26) Dirscherl, G., and König, B. (2008) The use of solid-phase synthesis techniques for the
9 preparation of peptide-metal complex conjugates. *Eur. J. Org. Chem.* 597-634.
10

11
12
13 (27) Metzler-Nolte, N. (2010) Biomedical applications of organometal-peptide conjugates. *Top.*
14 *Organomet. Chem.* 32, 195-217.
15

16
17
18 (28) Peindy N'Dongo, H. W., Ott, I., Gust, R., and Schatzschneider, U. (2009) Microwave-assisted
19 solid-phase synthesis, cellular uptake, and cytotoxicity studies of cymantrene-peptide bioconjugates. *J.*
20 *Organomet. Chem.* 694, 823-827.
21
22
23

24
25
26
27 (29) Gross, A., and Metzler-Nolte, N. (2009) Synthesis and characterization of a ruthenocenoyl
28 bioconjugate with the cyclic octapeptide octreotate. *J. Organomet. Chem.* 694, 1185-1188.
29

30
31
32 (30) van Rijt, S. H., Kostrhunova, H., Brabec, V., and Sadler, P. J. (2011) Functionalization of osmium
33 arene anticancer complexes with (Poly)arginine: effect on cellular uptake, internalization, and
34 cytotoxicity. *Bioconjugate Chem.* 22, 218-226.
35
36
37

38
39
40 (31) Puckett, C. A., and Barton, J. K. (2010) Targeting a ruthenium complex to the nucleus with short
41 peptides. *Bioorg. Med. Chem.* 18, 3564-3659.
42

43
44
45 (32) Splith, K., Hu, W., Schatzschneider, U., Gust, R., Ott, I., Onambele, L. A., Prokop, A., and
46 Neundorf, I. (2010) Protease-activatable organometal-peptide bioconjugates with enhanced cytotoxicity
47 on cancer cells. *Bioconjugate Chem.* 21, 1288-1296.
48
49

50
51
52 (33) Mukhopadhyay, S., Barnes, C. M., Haskel, A., Short, S. M., Barnes, K. R., and Lippard, S. J.
53 (2008) Conjugated platinum(IV)-peptide complexes for targeting angiogenic tumor vasculature.
54 *Bioconjugate Chem.* 19, 39-49.
55
56
57
58
59
60

1
2
3
4
5
6
7
8
9
10
11
12
13
14
15
16
17
18
19
20
21
22
23
24
25
26
27
28
29
30
31
32
33
34
35
36
37
38
39
40
41
42
43
44
45
46
47
48
49
50
51
52
53
54
55
56
57
58
59
60

(34) Hsieh, H.-P., Wu, Y.-T., Chen, S.-T., and Wang, K.-T. (1999) Direct solid-phase synthesis of octreotide conjugates: precursors for use as tumor-targeted radiopharmaceuticals. *Bioorg. Med. Chem.* *7*, 1797-1803.

(35) Moradell, S., Lorenzo, J., Rovira, A., Robillard, M. S., Aviles, F. X., Moreno, V., de Llorens, R., Martinez, M. A., Reedijk, J., and Llobet, A. (2003) Platinum complexes of diaminocarboxylic acids and their ethyl ester derivatives: the effect of the chelate ring size on antitumor activity and interactions with GMP and DNA. *J. Inorg. Biochem.* *96*, 493-502.

(36) van Rijt, S. H., Peacock, A. F. A., Johnstone, R. D. L., Parsons, S., and Sadler, P. J. (2009) Organometallic osmium(II) arene anticancer complexes containing picolinate derivatives. *Inorg. Chem.* *48*, 1753-1762.

(37) Hodson, E., and Simpson, S. J. (2004) Synthesis and characterization of $[(\eta^6\text{-cymene})\text{Ru}(\text{L})\text{X}_2]$ compounds: single crystal X-ray structure of $[(\eta^6\text{-cymene})\text{Ru}(\text{P}\{\text{OPh}\}_3)\text{Cl}_2]$ at 203 K. *Polyhedron* *23*, 2695-2707.

(38) Chaplin, A. B., and Dyson, P. J. (2007) Catalytic activity of bis-phosphine ruthenium(II)-arene compounds: Structure-activity correlations. *Organometallics* *26*, 2447-2455.

(39) Charvat, T. T., Lee, D. J., Robinson, W. E., and Chamberlin, A. R. (2006) Design, synthesis, and biological evaluation of chicoric acid analogs as inhibitors of HIV-1 integrase. *Bioorg. Med. Chem.* *14*, 4552-4567.

(40) Garipey, J., Remy, S., Zhang, X., Ballinger, J. R., Bolewska-Pedyczak, E., Rauth, M., and Bisland, K. (2002) A simple two-step approach for introducing a protected diaminedithiol chelator during solid-phase assembly of peptides. *Bioconjugate Chem.* *13*, 679-684.

(41) Marchán, V., Moreno, V., Pedroso, E., and Grandas, A. (2001) Towards a better understanding of the cisplatin mode of action. *Chem. Eur. J.* *7*, 808-815.

1 (42) Marchán, V., Pedroso, E., and Grandas, A. (2004) Insights into the reaction of transplatin with
2 DNA and proteins: Methionine-mediated formation of histidine-guanine trans-Pt(NH₃)₂ cross-links.
3
4
5 *Chem. Eur. J.* *10*, 5369-5375.
6

7
8 (43) Algueró, B., López de la Osa, J., González, C., Pedroso, E., Marchán, V., and Grandas, A. (2006)
9 Selective platination of modified oligonucleotides and duplex cross-links. *Angew. Chem. Int. Ed.* *45*,
10
11
12 8194-8197.
13

14
15
16 (44) Goddard, D. T., and Kneller, G. SPARKY (University of California, San Francisco).
17

18
19 (45) Singh, S. K., Trivedi, M., Chandra, M., Sahay, A. N., and Pandey, D. S. (2004) Luminescent
20 piano-stool complexes incorporating 1-(4-cyanophenyl)imidazole: Synthesis, spectral, and structural
21
22
23 studies. *Inorg. Chem.* *43*, 8600-8608.
24
25

26
27 (46) Koradi, R., Billeter, M., and Wuthrich, K. (1996) MOLMOL: a program for display and analysis
28
29
30 of macromolecular structures. *J. Mol. Graphics* *14*, 29-32.
31

32
33 (47) Peacock, A. F. A., Parsons, S., and Sadler, P. J. (2007) Tuning the hydrolytic aqueous chemistry
34
35
36 of osmium arene complexes with *N,O*-chelating ligands to achieve cancer cell cytotoxicity. *J. Am.*
37
38
39 *Chem. Soc.* *129*, 3348-3357.
40

41 (48) van Rijt, S. H., Mukherjee, A., Pizarro, A. M., and Sadler, P. J. (2010) Cytotoxicity,
42
43
44 hydrophobicity, uptake, and distribution of osmium(II) anticancer complexes in ovarian cancer cells. *J.*
45
46
47 *Med. Chem.* *53*, 840-849.
48

49 (49) Morris, R. E., Aird, R. E., Murdoch, P. del S., Chen, H., Cummings, J., Hughes, N. D., Parsons,
50
51
52 S., Parkin, A., Boyd, G., Jodrell, D. I., and Sadler, P. J. (2001) Inhibition of cancer cell growth by
53
54
55 ruthenium(II) arene complexes. *J. Med. Chem.* *44*, 3616-3621.
56

57 (50) Moreno, V., Font-Bardia, M., Calvet, T., Lorenzo, J., Aviles, F. X., Garcia, M. H., Morais, T. S.,
58
59
60 Valente, A., and Robalo, M. P. (2011) DNA interaction and cytotoxicity studies of new ruthenium(II)

1 cyclopentadienyl derivative complexes containing heteroaromatic ligands. *J. Inorg. Biochem.* 105, 241-
2 249.
3

4
5 (51) Gianferrara, T., Bratsos, I., and Alessio, E. (2009) A categorization of metal anticancer
6 compounds based on their mode of action. *Dalton Transactions*, 37, 7588-7598.
7

8
9 (52) Jennerwein, M., and Andrews, P. A. (1995) Effect of intracellular chloride on the cellular
10 pharmacodynamics of cis-diamminedichloroplatinum(II). *Drug Metab. Dispos.* 23, 178-184.
11

12
13 (53) Wang, F., Habtemariam, A., van der Geer, E. P. L., Fernandez, R., Melchart, M., Deeth, R. J.,
14 Aird, R., Guichard, S., Fabbiani, F. P. A., Lozano-Casal, P., Oswald, I. D. H., Jodrell, D. I., Parsons, S.,
15 and Sadler, P. J. (2005) Controlling ligand substitution reactions of organometallic complexes: Tuning
16 cancer cell cytotoxicity. *Proc. Nat. Acad. Sci. USA* 102, 18269-18274.
17

18
19 (54) Peacock, A. F. A., Habtemariam, A., Moggach, S. A., Prescimone, A., Parsons, S., and Sadler, P.
20 J. (2007) Chloro half-sandwich osmium(II) complexes: influence of chelated *N,N*-ligands on hydrolysis,
21 guanine binding, and cytotoxicity. *Inorg. Chem.* 46, 4049-4059.
22

23
24 (55) Novakova, O., Chen, H., Vrana, O., Rodger, A., Sadler, P. J., and Brabec, V. (2003) DNA
25 Interactions of monofunctional organometallic ruthenium(II) antitumor complexes in cell-free media.
26 *Biochemistry* 42, 11544-11554.
27

28
29 (56) Liu, H.-K., Wang, F., Parkinson, J. A., Bella, J., and Sadler, P. J. (2006) Ruthenation of duplex
30 and single-stranded d(CGGCCG) by organometallic anticancer complexes. *Chem. Eur. J.* 12, 6151-
31 6165.
32

33
34 (57) Gossens, C., Tavernelli, I., and Rothlisberger, U. (2009) Binding of organometallic ruthenium(II)
35 anticancer compounds to nucleobases: A computational study. *J. Phys. Chem. A* 113, 11888-11897.
36
37
38
39
40
41
42
43
44
45
46
47
48
49
50
51
52
53
54
55
56
57
58
59
60

1 (58) Kostrhunova, H., Florian, J., Novakova, O., Peacock, A. F. A., Sadler, P. J., and Brabec, V. (2008)
2 DNA Interactions of monofunctional organometallic osmium(II) antitumor complexes in cell-free
3 media. *J. Med. Chem.* 51, 3635-3643.
4
5

6
7
8 (59) Fischer, R., Mader, O., Jung, G., and Brock, R. (2003) Extending the applicability of
9 carboxyfluorescein in solid-phase synthesis. *Bioconjugate Chem.* 14, 653-660.
10
11

12
13 (60) Watson, J.C., Balster, D.A., Gebhardt, B.M., O'Dorisio, T.M., O'Dorisio, M.S., Espenan, G.D.,
14 Drouant, G.J., and Woltering, E.A. (2001) Growing vascular endothelial cells express somatostatin
15 subtype 2 receptors. *Br. J. Cancer* 85, 266-272.
16
17

18
19
20
21 (61) Hornick, C. A., Anthony, C.T., Hughey, S., Gebhardt, B.M., Espenan, G.D., and Woltering, E.A.
22 (2000) Progressive nuclear translocation of somatostatin analogs. *J. Nucl. Med.* 41, 1256-1263.
23
24

25
26
27 (62) Zhang, Y., Wang, X., Wang, J., Zhang, X., and Zhang, Q. (2011) Octreotide-modified polymeric
28 micelles as potential carriers for targeted docetaxel delivery to somatostatin receptor overexpressing
29 tumor cells. *Pharm. Res.* 28, 1167-1178.
30
31

32
33
34
35 (63) Huang, C.M., Wu, Y. T., and Chen, S.T. (2000) Targeting delivery of paclitaxel into tumor cells
36 via somatostatin receptor endocytosis. *Chem. Biol.* 7, 453-461.
37
38

39
40 (64) Wynants, C., Van Binst, G., and Loosli, H. R. (1985) SMS 201-995, a very potent analogue of
41 somatostatin. Assignment of the ^1H 500 MHz n.m.r. spectra and conformational analysis in aqueous
42 solution. *Int. J. Peptide Protein Res.* 25, 608-614.
43
44

45
46
47
48 (65) Wynants, C., Van Binst, G., and Loosli, H. R. (1985) SMS 201-995, an octapeptide somatostatin
49 analogue. Assignment of the ^1H 500 MHz n.m.r. spectra and conformational analysis of SMS 201-995
50 in dimethylsulfoxide. *Int. J. Peptide Protein Res.* 25, 615-621.
51
52
53
54
55
56
57
58
59
60

1 (66) Melacini, G., Zhu, Q., and Goodman, M. (1997) Multiconformational NMR Analysis of
2 sandostatin (octreotide): equilibrium between β -sheet and helical structures. *Biochemistry* 36, 1233-
3 1241.
4
5

6
7
8 (67) Deshmukh, M. V., Voll, G., Kuehlewein, A., Maecke, H., Schmitt, J., Kessler, H., and
9 Gemmecker, G. (2005) NMR studies reveal structural differences between the Gallium and Yttrium
10 complexes of DOTA-D-Phe1-Tyr3-octreotide. *J. Med. Chem.* 48, 1506-1514.
11
12

13
14
15 (68) Reubi, J.C., Schar, J.C., Waser, B., Wenger, S., Heppeter, A., Schmitt, J.S., and Mäcke, H.R.
16 (2000) Affinity profiles for human somatostatin receptor subtypes sstr1-sstr5 of somatostatin
17 radiotracers selected for scintigraphic and radiotherapeutic use. *Eur. J. Nucl. Med.* 27, 273-282.
18
19
20

21
22 (69) Zhang, J., Jin, W., Wang, X., Wang, J., Zhang, X., and Zhang, Q. (2010) A novel octreotide
23 modified lipid vesicle improved the anticancer efficacy of doxorubicin in somatostatin receptor 2
24 positive tumor models. *Mol Pharm.* 7, 1159-1168.
25
26
27
28

29
30 (70) Cascini, G. L., Cuccurullo, V., and Mansi, L. (2010) The non tumour uptake of (111)In-octreotide
31 creates new clinical indications in benign diseases, but also in oncology. *Q. J Nucl Med Mol Imaging* 54,
32 24-36.
33
34
35
36
37
38
39
40
41
42
43
44
45
46
47
48
49
50
51
52
53
54
55
56
57
58
59
60

TABLE OF CONTENTS (TOC)

